in mice and tumor accumulativeness in tumor-bearing mice. In addition, we confirmed that multiple injections affect the biodistribution characteristics of the second dose of PEGylated KG6. The unfavorable biodistribution properties of intact KG6, such as rapid elimination from the blood and non-specific uptake by the liver and kidney, could be improved by modification with PEG chains. In addition, PEG(76)-KG6 was significantly accumulated in tumor via the EPR effect, whereas the intact KG6 showed no significant accumulation. Moreover, compared with a single administration, the biodistribution characteristics of the second dose of PEGylated KG6 showed no change on multiple injections. These results suggest the PEGylated lysine dendrimers to be useful as a base material for a clinically applicable tumor-targeting drug carrier.

Acknowledgements

This work was supported in part by Grant-in-Aids for Scientific Research from the Ministry of Education, Culture, Sports, Science, and Technology of Japan, and by the Health and Labour Sciences Research Grants for Research on Advanced Medical Technology from the Ministry of Health, Labour and Welfare of Japan.

References

[1] N.D. James, R.J. Coker, D. Tomlinson, J.R. Harris, M. Gompels, A.J. Pinching, J.S. Stewart, Liposomal doxorubicin (Doxil): an effective new treatment for Kaposi's sarcoma in AIDS, Clin. Oncol. (R. Coll. Radiol.) 6 (1994) 294–296.

[2] D.S. Alberts, D.J. Garcia, Safety aspects of pegylated liposomal doxorubicin in patients with cancer, Drugs 54 (1997) 30–35.

[3] R. Esfand, D.A. Tomalia, Poly(amidoamine) (PAMAM) dendrimers: from biomimicry to drug delivery and biomedical applications, Drug Discov. Today 6 (2001) 427–436.

[4] S.E. Stiriba, H. Frey, R. Haag, Dendritic polymers in biomedical applications: from potential to clinical use in diagnostics and therapy, Angew. Chem., Int. Ed. 41 (2002) 1329–1334.

[5] J.F. Kukowska-Latallo, K.A. Candido, Z. Cao, S.S. Nigavekar, I.J. Majoros, T.P. Thomas, L.P. Balogh, M.K. Kahn, J.R. Baker Jr., Nanoparticle targeting of anticancer drug improves therapeutic response in animal model of human epithelial cancer, Cancer Res. 65 (2005) 5317–5324.

[6] H. Yoo, R.L. Juliano, Enhanced delivery of antisense oligonucleotides with fluorophore-conjugated PAMAM dendrimers, Nucleic Acids Res. 28 (2000) 4225–4231.

[7] J.S. Choi, K. Nam, J.Y. Park, J.B. Kim, J.K. Lee, J.S. Park, Enhanced transfection efficiency of PAMAM dendrimer by surface modification with *L*-arginine, J. Control. Release 99 (2004) 445–456.

[8] K. Wada, H. Arima, T. Tsutsumi, F. Hirayama, K. Uekama, Enhancing effects of galactosylated dendrimer/alpha-cyclodextrin conjugates on gene transfer efficiency, Biol. Pharm. Bull. 28 (2005) 500–505.

[9] H. Kobayashi, S. Kawamoto, R.A. Star, T.A. Waldmann, Y. Tagaya, M.W. Brechbiel, Micro-magnetic resonance lymphangiography in mice using a novel dendrimer-based magnetic resonance imaging contrast agent, Cancer Res. 63 (2003) 271–276.

[10] H. Kobayashi, S.K. Jo, S. Kawamoto, H. Yasuda, X. Hu, M.V. Knopp, M.W. Brechbiel, P.L. Choyke, R.A. Star, Polyamine dendrimer-based MRI contrast agents for functional kidney imaging to diagnose acute renal failure, J. Magn. Reson. Imaging 20 (2004) 512–518.

[11] N. Malik, R. Wiwattanapatapee, R. Klopsch, K. Lorenz, H. Frey, J.W. Weener, E.W. Meijer, W. Paulus, R. Duncan, Dendrimers: relationship between structure and biocompatibility in vitro, and preliminary studies on the biodistribution of ^{125}I-labelled polyamidoamine dendrimers in vivo, J. Control. Release 65 (2000) 133–148.

[12] M. Ohsaki, T. Okuda, A. Wada, T. Hirayama, T. Niidome, H. Aoyagi, *In vitro* gene transfection using dendritic poly(*L*-lysine), Bioconjug. Chem. 13 (2002) 510–517.

[13] T. Okuda, A. Sugiyama, T. Niidome, H. Aoyagi, Characters of dendritic poly(*L*-lysine) analogues with the terminal lysines replaced with arginines and histidines as gene carriers *in vitro*, Biomaterials 25 (2004) 537–544.

[14] T. Okuda, S. Kawakami, T. Maeie, T. Niidome, F. Yamashita, M. Hashida, Biodistribution characteristics of amino acid dendrimers and their PEGylated derivatives after intravenous administration, J. Control. Release 114 (2006) 69–77.

[15] C.G. Fields, D.H. Lloyd, R.L. Macdonald, K.M. Otteson, R.L. Noble, HBTU activation for automated Fmoc solid phase peptide synthesis, Pept. Res. 4 (1991) 95–101.

[16] D. Hnatowich, W.W. Layne, R.L. Childs, The preparation and labeling of DTPA-coupled albumin, J. Appl. Radiat. Isot. 12 (1982) 327–332.

[17] B. Skoog, Determination of polyethylene glycols 4000 and 6000 in plasma protein preparations, Vox Sang. 37 (1979) 345–349.

[18] J.R. Duncan, M.J. Welch, Intracellular metabolilsm of indium-111-DTPA-labeled receptor targeted proteins, J. Nucl. Med. 34 (1993) 1728–1738.

[19] F. Staud, M. Nishikawa, K. Morimoto, Y. Takakura, M. Hashida, Disposition of radioactivity after injection of liver-targeted proteins labeled with ^{111}In or ^{125}I. Effect of labeling on distribution and excretion of radioactivity in rats, J. Pharm. Sci. 88 (1999) 577–585.

[20] T. Ishida, M. Harada, X.Y. Wang, M. Ichihara, K. Irimura, H. Kiwada, Accelerated blood clearance of PEGylated liposomes following preceding liposome injection: effects of lipid dose and PEG surface-density and chain length of the first-dose liposomes, J. Control. Release 105 (2005) 305–317.

[21] Y. Matsumura, H. Maeda, A new concept for macromolecular therapeutics in cancer chemotherapy: mechanism of tumoritropic accumulation of proteins and the antitumor agent smancs, Cancer Res. 46 (1986) 6387–6392.

[22] T. Nakanishi, S. Fukushima, K. Okamoto, M. Suzuki, Y. Matsumura, M. Yokoyama, T. Okano, Y. Sakurai, K. Kataoka, Development of the polymer micelle carrier system for doxorubicin, J. Control. Release 74 (2001) 295–302.

[23] A.N. Lukyanov, W.C. Heartner, V.P. Torchilin, Increased accumulation of PEG-PE micelles in the area of experimental myocardial infarction in rabbits, J. Control. Release 97 (2004) 187–193.

[24] Y. Bae, N. Nakanishi, S. Fukushima, H. Koyama, M. Yasuhiro, K. Kataoka, Preparation and biological characterization of polymeric micelle drug carriers with intracellular pH-triggered drug release properties: tumor permeability, controlled subcellular drug distribution, and enhanced in vivo antitumor efficacy, Bioconjug. Chem. 16 (2005) 122–130.

[25] O. Ishida, K. Maruyama, H. Tanahashi, M. Iwatsuru, K. Sasaki, M. Eriguchi, H. Yanagie, Liposomes bearing polyethyleneglycol-coupled transferrin with intracellular targeting property to the solid tumor in vivo, Pharm. Res. 18 (2001) 1042–1048.

[26] Y. Matsumura, M. Gotoh, K. Muro, Y. Yamada, K. Shirao, Y. Shimada, M. Okuwa, S. Matsumoto, Y. Miyata, H. Ohkura, K. Chin, S. Baba, T. Yamao, A. Kannami, Y. Takamatsu, K. Ito, K. Takahashi, Phase I and phamacokinetic study of MCC-465, a doxorubicin (DXR) encapsulated in PEG immunoliposome, in patients with metastatic stomach cancer, Ann. Oncol. 15 (2004) 517–525.

[27] E.T. Dams, P. Laverman, W.J. Oyen, G. Storm, G.L. Scherphof, J.W. van Der Meer, F.H. Corstens, O.C. Boerman, Accelerated blood clearance and altered biodistribution of repeated injections of sterically stabilized liposomes, J. Pharmacol. Exp. Ther. 292 (2000) 1071–1079.

[28] T. Ishida, T. Ichikawa, M. Ichihara, Y. Sadzuka, H. Kiwada, Effect of the physicochemical properties of initially injected liposomes on the clearance of subsequently injected PEGylated liposomes in mice, J. Control. Release 95 (2004) 403–412.

Intracellular Trafficking Is the Important Process That Determines the Optimal Charge Ratio on Transfection by Galactosylated Lipoplex in HepG2 Cells

Yasunori SAITO, Shigeru KAWAKAMI, Yoshiyuki YABE, Fumiyoshi YAMASHITA, and Mitsuru HASHIDA*

Department of Drug Delivery Research, Graduate School of Pharmaceutical Sciences, Kyoto University; Sakyo-ku, Kyoto 606–8501, Japan. Received May 23, 2006; accepted June 22, 2006; published online June 26, 2006

The purpose of the present study was to gain insight into the major factors affecting transfection efficiency with galactosylated lipoplex in HepG2 cells. In this study, lipoplex and galactosylated lipoplex were examined at different charge ratios (− : +): 1.0 : 1.2, 1.0 : 2.3, 1.0 : 3.1, 1.0 : 4.7, and 1.0 : 7.0. The particle size and zeta potential of the both lipoplexes was dependent on the charge ratio. Cellular uptake was evaluated by using [^{32}P]-labeled pCMV-Luc and this showed that the cellular uptake of galactosylated lipoplex was significantly higher than that of lipoplex at a charge ratio ranging from 1.0 : 2.3 to 1.0 : 7.0. As the charge ratio increased in both lipoplexes, the apparent cellular uptake increased. Transfection activity by galactosylated lipoplex was significantly higher than that by lipoplex except at a charge ratio of 1.0 : 7.0. The optimal charge ratio for transfection efficacy was 1.0 : 2.3 and transfection was reduced at higher charge ratios. Both lipoplexes exhibited no significant cytotoxicity at any charge ratio. In conclusion, it is suggested that intracellular trafficking, rather than the degree of uptake and cytotoxicity, is the important process that determines the optimal charge ratio of galactosylated lipoplex in HepG2 cells.

Key words gene delivery; hepatocytes; targeting; liposome; lipoplex

Non-viral vectors have advantages in terms of their simplicity of use and ability to be produced on a large scale if necessary. Among various types of non-viral vectors, cationic liposome-mediated gene transfection is one of the most promising approaches due to the high transfection efficiency.[1—4] Gene delivery to hepatocytes is of great therapeutic potential, since the cells are responsible for the synthesis of a wide variety of proteins that play important biological roles both inside and outside the liver. To achieve targeted gene delivery to hepatocytes, galactose has been shown to be a promising targeting ligand because these cells possess a large number of asialoglycoprotein receptors that recognize the galactose units on the synthetic galactosylated carriers.[5—7] Recently, we have developed galactosylated cationic liposomes containing cholesten-5-yloxy-*N*-(4-((1-imino-2-D-thiogalactosylethyl)amino)butyl)formamide (Gal-C4-Chol) for hepatocyte-selective gene transfection *via* asialoglycoprotein receptor-mediated endocytosis after intraportal administration into mice.[8—10] In this approach, plasmid DNA is mixed with preformed galactosylated cationic liposomes to form galactosylated lipoplex, based on electrostatic interaction, which can then interact with hepatocytes and be taken up by them. Since Gal-C4-Chol possesses an imino group for binding to plasmid DNA *via* electrostatic interaction, many galactose units can be introduced on the liposomal surface without loss of binding affinity to plasmid DNA. These promising properties of our galactosylated lipoplex enable hepatocyte-selective gene transfer to be achieved under *in vivo* conditions. The overall ratio of the positive charge on a cationic lipid to the negative charge on a plasmid DNA seems to be a critical determinant of this phenomenon. It is generally accepted that the physicochemical characteristics of the galactosylated lipoplex prepared at different mixing ratios are so different that their cellular uptake, subsequent intracellular trafficking and resultant transfection efficiency would be significantly affected. However, there is little published information on the relationship between these physicochemical and biological factors in the lipoplex and/or galactosylated lipoplex.

Previously, we have investigated the effect of the pDNA-*N*-[1-(2,3-dioleyloxy)propyl]-*N*,*N*,*N*-trimethylammonium chloride (DOTMA)/dioleoylphosphatidylethanolamine (DOPE) liposomes mixing (charge) ratio on the particle size, zeta potential and structure of the lipoplex, which directly affects cellular uptake, intracellular distribution of the complex, and the subsequent gene expression efficiency. And we have demonstrated that the mixing (charge) ratio of plasmid DNA complexed with DOTMA/DOPE liposomes significantly affects the intracellular trafficking, which is an important determinant of the optimal charge ratio in cationic liposome-mediated transfection.[11] The *in vivo* gene transfection efficacy by lipoplex was markedly affected by the type of neutral lipid. Previously, we have demonstrated that the transfection efficacy of cholesterol containing galactosylated cationic liposomes (DOTMA/cholesterol/Gal-C4-Chol) in hepatocytes was markedly higher than that of DOPE, which is a pH-sensitive lipid,[12] containing galactosylated cationic liposomes (DOPE/Gal-C4-Chol) after intraportal administration.[8] In order to achieve a more efficient gene carrier system, the limiting processes for gene expression needed to be investigated. However, the relationships involved in cholesterol-containing galactosylated cationic liposome-mediated gene transfer, cellular binding and uptake and intracellular trafficking are not yet fully understood.

In the present study, transfection efficiencies of galactosylated lipoplex were evaluated using cultured cells in relation to their physicochemical properties. Then, the cellular uptake, intracellular trafficking and cytotoxicity of galactosylated lipoplex were also examined in human hepatoma HepG2 cells, which are known to express asialoglycoprotein

* To whom correspondence should be addressed. e-mail: hashidam@pharm.kyoto-u.ac.jp

receptors. It is suggested that intracellular trafficking, rather than the degree of uptake and cytotoxicity, is the important process that determines the optimal charge ratio of galactosylated lipoplex in HepG2 cells. pCMV-Luc was selected as a model plasmid DNA for evaluating the gene expression by luciferase. DOTMA/cholesterol liposomes and DOTMA/cholesterol/Gal-C4-Chol liposomes were selected as control cationic liposomes and galactosylated cationic liposomes, respectively.

MATERIALS AND METHODS

Materials *N*-(4-Aminobutyl) carbamic acid *tert*-butyl ester and DOTMA were obtained from Tokyo Kasei Kogyo Co., Ltd. (Tokyo, Japan). Cholesterol was obtained from Nacalai Tesque, Inc. (Kyoto, Japan). Cholesterol test-E Wako was purchased from Wako Pure Chemical Industries, Ltd. (Osaka, Japan). Cholesteryl chloroformate was obtained from Sigma Chemicals, Inc. (St. Louis, MO, U.S.A.). Dulbecco's modified Eagle's minimum essential medium (DMEM). Fetal bovine serum (FBS) was obtained from Biowhittaker (Walkersville, MD, U.S.A.). Opti-MEM I® and other culture reagents were obtained from Gibco BRL (Grand Island, NY, U.S.A.). All other chemicals were of the highest purity available.

Construction and Preparation of Plasmid DNA (pCMV-Luc) pCMV-Luc was constructed by subcloning the *Hin*dIII/*Xba*I firefly luciferase cDNA fragment from pGL3-control vector (Promega Co., Madison, WI, U.S.A.) into the polylinker of pcDNA3 vector (Invitrogen, Carlsbad, CA, U.S.A.). Plasmid DNA was amplified in the *Escherichia coli* strain DH5a, isolated, and purified using a QIAGEN Endofree Plasmid Giga Kit (QIAGEN GmbH, Hilden, Germany). Purity was confirmed by 1% agarose gel electrophoresis followed by ethidium bromide staining and the plasmid DNA concentration was measured by UV absorption at 260 nm.

Synthesis of Gal-C4-Chol Gal-C4-Chol was synthesized as reported previously.[13] Briefly, cholesteryl chloroformate and *N*-(4-aminobutyl)carbamic acid *tert*-butyl ester were reacted in chloroform for 24 h at room temperature. A solution of trifluoroacetic acid and chloroform was added dropwise and the mixture was stirred for 4 h at 4 °C. The solvent was evaporated to obtain *N*-(4-aminobutyl)-(cholesten-5-yloxyl)formamide which was then combined with 2-imino-2-methoxyethyl-1-thiogalactoside and the mixture was stirred for 24 h at 37 °C. After evaporation, the resultant material was suspended in water, dialyzed against distilled water for 48 h (12 kDa cut-off dialysis tubing), and then lyophilized.

Preparation of Galactosylated Cationic Liposomes Galactosylated cationic liposomes were prepared as reported previously.[8,10] The mixtures of DOTMA, cholesterol, and Gal-C4-Chol were dissolved in chloroform at a molar ratio of 2 : 1 : 1 for galactosylated cationic liposomes, vacuum-desiccated, and resuspended in sterile 5% dextrose solution at a concentration of 1 mg total lipids per ml. The suspension was sonicated for 3 min and the resulting liposomes were extruded 5-times through 0.45 μm polycarbonate membrane filters. The concentration of liposomes was adjusted by measuring the cholesterol concentration using the cholesterol test-E Wako.

Preparation of Lipoplex and Galactosylated Lipoplex The lipoplex and galactosylated lipoplex were prepared as reported previously.[8,10] Briefly, pDNA in sterile 5% dextrose solution was mixed with an equal volume of (galactosylated) cationic liposomes and incubated for 30 min. The mixing ratio of liposomes and pDNA was expressed as a charge ratio, which is the molar ratio of cationic lipids to pDNA phosphate residues.[14]

Evaluation of Physicochemical Properties The lipoplex and galactosylated lipoplex were dissolved at a plasmid DNA concentration of up to 1 μg/ml, and then their particle size and zeta-potential were measured by Zetasizer Nano ZS (Malvern Instruments Ltd., U.K.).

Uptake Experiment HepG2 cells were obtained from American Type Culture Collection (Manassas, VA, U.S.A.) and maintained in DMEM supplement with 10% FBS at 37 °C under an atmosphere of 5% CO_2 in air. The cells were plated on a 6-well cluster dish at a density of 2×10^5 cells/10.5 cm^2 and cultivated in 2 ml DMEM supplement with 10% FBS. Twenty-four hours later, the culture medium was replaced with an equivalent volume of HBSS containing 1 kBq/ml [^{32}P] plasmid DNA, 1 μg/ml cold plasmid DNA and cationic liposomes. After incubation for 3 h at 4 or 37 °C for given time periods, the solution was immediately removed by aspiration, the cells were washed 5-times with ice-cold HBSS buffer and solubilized in 1 ml 0.3 N NaOH solution with 10% Triton X-100. The radioactivity was measured by liquid scintillation counting (LSC-500, Beckman, Tokyo, Japan). The radioactivity data were normalized with respect to the protein contents of the cells. The protein content was determined by a modification of the Lowry method using Protein Quantification Kit (Dojindo Molecular Technologies, Inc., Gaithersburg, MD, U.S.A.).

Transfection Experiment The HepG2 cells were plated on a 6-well cluster dish at a density of 2×10^5 cells/10.5 cm^2 and cultivated in 2 ml DMEM supplemented with 10% FBS. After 24 h, the culture medium was replaced with Opti-MEM I® containing 1 μg/ml plasmid DNA and cationic liposomes. Six hours later, the incubation medium was replaced again with DMEM supplement with 10% FBS and incubated for an additional 42 h. Then, the cells were scraped off and suspended in 200 μl pH 7.4 phosphate-buffered saline (PBS). One hundred microliters cell suspension was subjected to three cycles of freezing (liquid N_2 for 3 min) and thawing (37 °C for 3 min), followed by centrifugation at 10000 ***g*** for 3 min. The supernatants were stored at −20 °C until the luciferase assays were performed. Ten microliters supernatant was mixed with 100 μl luciferase assay buffer (Picagene, Toyo Ink, Tokyo, Japan) and the light produced was immediately measured using a luminometer (Lumat LB 9507, EG & G Berthold, Bad Wildbad, Germany). The activity is indicated as the relative light units per mg protein. The radioactivity data were normalized with respect to the protein content of the cells. The protein content of the cell suspension in PBS was determined by a modified Lowry method using Protein Quantification Kit (Dojindo Molecular Technologies, Inc., Gaithersburg, MD, U.S.A.).

Cytotoxicity Experiment Cytotoxicity was evaluated by MTT assay. The cells, plated on a 24-well plate at a density of 0.38×10^5 cells/2.0 cm^2, were incubated in 500 μl Opti-MEM I® containing 1 μg/ml plasmid DNA and cationic lipo-

somes. Six hours later, the incubation medium was replaced with DMEM supplement with 10% FBS and incubated for an additional 42 h. After addition of 0.5 mg/ml MTT solution, the solution was incubated overnight at 37 °C with 10% SDS solution. The absorbance was measured at test and reference wavelengths of 570 and 660 nm, respectively, in a two-wavelength microplate photometer (Bio-Rad Model 450, Hercules, CA, U.S.A.).

Statistical Analysis Statistical analysis was performed using Student's paired *t*-test for two groups and the Tukey–Kramer test for multiple comparisons between groups. $p<0.05$ was considered to be indicative of statistical significance.

RESULTS

Physicochemical Properties of Galactosylated Lipoplex The particle size and the zeta potential of the both lipoplex and galactosylated lipoplex were examined at different charge ratios. The particle size and zeta potential of both lipoplexes depended on the charge ratio (Figs. 1, 2). The particle size was about 200 nm at a charge ratio of 1.0 : 1.2 and the particle size increased in parallel with the ratio and then decreased at higher charge ratios. The zeta potential of both the lipoplex and galactosylated lipoplex also depended on the charge ratio (Fig. 2). The zeta potential was −4 mV at a charge ratio of 1.0 : 1.2 and became positive at a charge ratio of 1.0 : 1.6 (about+40 mV). At a charge ratio of 1.0 : 7.5, both the lipoplex and galactosylated lipoplex exhibited a positive zeta potential (about+60 mV).

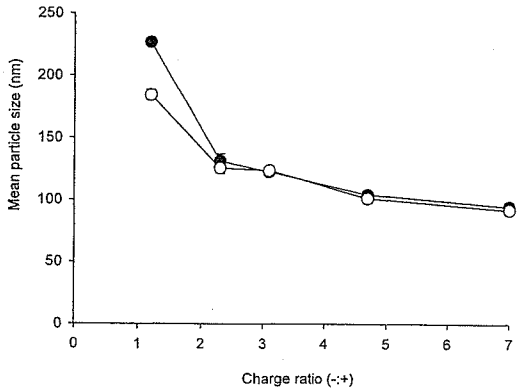

Fig. 1. The Mean Particle Size of the Lipoplex (Open Circle) and Galactosylated Lipoplex (Closed Circle) at Different Charge Ratios

The mean particle size was plotted as a function of the charge ratio. Error bars represent standard deviations.

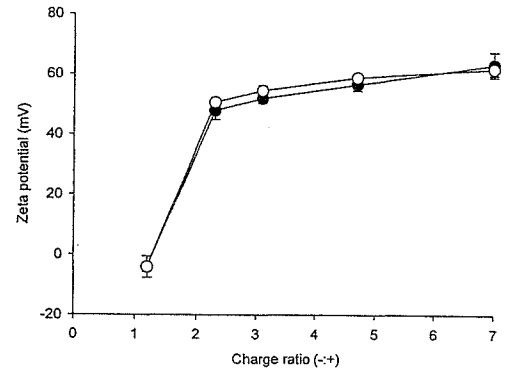

Fig. 2. The Zeta Potential of the Lipoplex (Open Circle) and Galactosylated Lipoplex (Closed Circle) at Different Charge Ratios

The zeta potential was plotted as a function of the charge ratio. Error bars represent standard deviations.

Uptake Characteristics of Galactosylated Lipoplex In order to investigate a possible correlation between the cellular uptake of lipoplex and subsequent gene expression, the cellular association of the lipoplex containing ^{32}P-labeled plasmid DNA was evaluated at 4 and 37 °C at different charge ratios (Fig. 3). Cellular uptake of galactosylated lipoplex was significantly higher than that of lipoplex at a charge ratio (− : +) from 1.0 : 2.3 to 1.0 : 7.0. As the charge ratio increased in both lipoplexes, the apparent cellular association at both temperatures increased. At a charge ratio (− : +) of 1.0 : 1.2, on the other hand, the apparent cellular uptake by galactosylated lipoplex was similar to that by lipoplex.

Transfection Characteristics of Galactosylated Lipoplex HepG2 cells were selected for transfection with the lipoplex or galactosylated lipoplex prepared at different charge ratios (Fig. 4). Extremely large differences in the gene expression level were observed at different charge ratios. Transfection activity by galactosylated lipoplex was significantly higher than that by lipoplex at a charge ratio (− : +) of 1.0 : 1.2 to 1.0 : 4.7. The optimal charge ratio (− : +) for transfection efficacy in both lipoplexes was 1.0 : 2.3 and transfection was reduced at higher charge ratios. In contrast, transfection efficacy of both lipoplexes was almost identical when they were prepared at a charge ratio (− : +) of 1.0 : 7.0.

Internalization and Transfection Efficacy per Internalization amount of Galactosylated Lipoplex We roughly

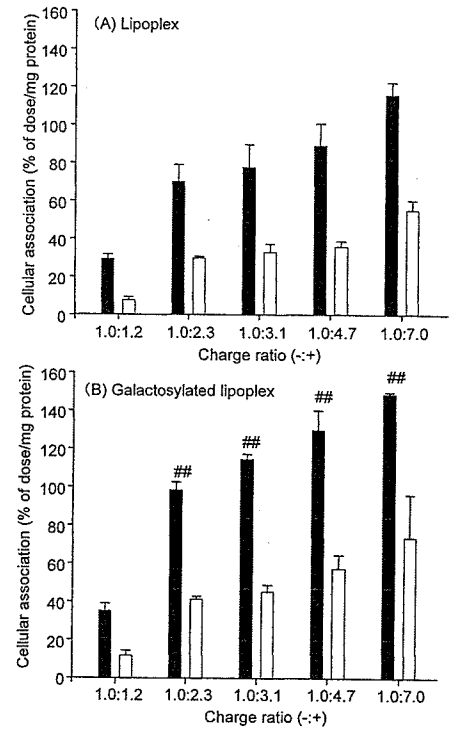

Fig. 3. Cellular Association at 37 °C (Filled Bar) and 4 °C (Open Bar) of [^{32}P]-Labeled-Plasmid DNA Lipoplex and Galactosylated Lipoplex at Different Charge Ratios after 3 h incubation in HepG2 cells

Error bars represent standard deviations. Statistically significant differences from lipoplex at 37 °C (## $p<0.01$).

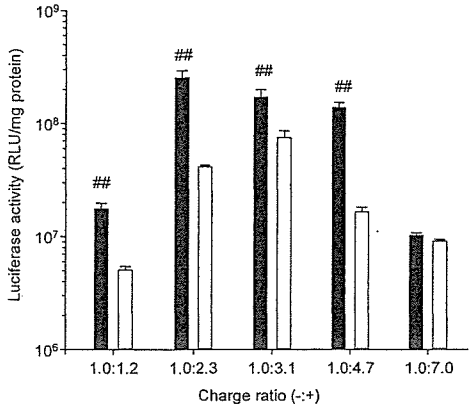

Fig. 4. Transfection Activity after Transfection by Lipoplex (Open Bar) and Galactosylated Lipoplex (Closed Bar) at Different Charge Ratio in HepG2 Cells

Error bars represent standard deviations. Statistically significant differences from lipoplex (## $p<0.01$).

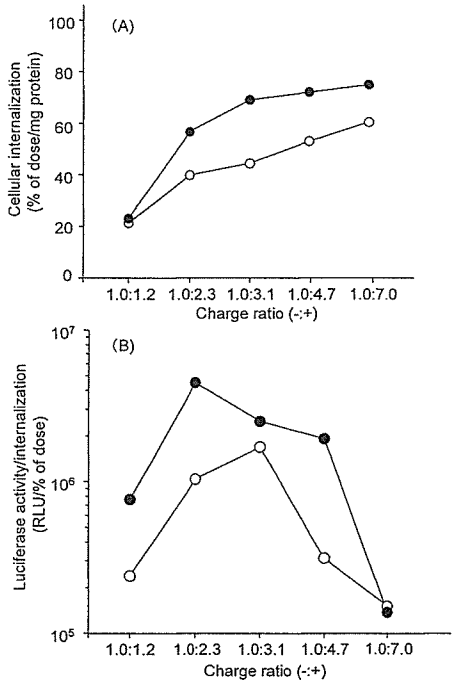

Fig. 5. Cellular Internalization (A) and Luciferase Activity/Cellular Internalization (B) after Transfection by Lipoplex (Open Bar) and Galactosylated Lipoplex (Closed Bar) at Different Charge Ratio in HepG2 Cells

Cellular internalization was calculated by the difference in the amount of [^{32}P]-labeled-plasmid DNA cellular association between 37 °C and 4 °C.

estimated the amount of internalized plasmid DNA by subtracting the amount of adsorbed plasmid DNA on the cell surface at 4 °C from the amount of cell-associated plasmid DNA at 37 °C, assuming that the amounts adsorbed at both temperatures were the same. The calculated amount of plasmid DNA taken up by the cells also increased as the charge ratio (− : +) of both lipoplexes increased (Fig. 5A). Then, luciferase activity was dividing by internalization amount. The transfection efficacy per internalization amount of galactosylated lipoplex and lipoplex was the highest at the charge ratio (− : +) of 1.0 : 2.3 and 1.0 : 3.1, respectively (Fig. 5B).

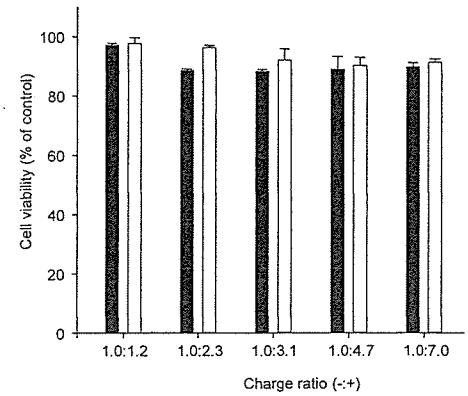

Fig. 6. Cytotoxic Effect after Transfection by Lipoplex (Open Bar) and Galactosylated Lipoplex (Closed Bar) at Different Charge Ratio in HepG2 Cells

Cell growth was measured by MTT assay. Data represent the % of cell growth compared with untreated cells. Error bars represent standard deviations.

Cytotoxicity of Galactosylated Lipoplex To assess the relationship between cytotoxicity and gene expression efficiency, the cytotoxic effects of both lipoplexes were examined by MTT assay. Although there was a slight reduction in the amounts of formazan crystals in the cells, both lipoplexes exhibited no significant toxicity at any charge ratio (Fig. 6). There were no significant differences in the protein level and cell viability between these charge ratios after a 48 h incubation (data not shown).

DISCUSSION

The purpose of the present study was to investigate the major factors affecting transfection efficiency with galactosylated lipoplex in HepG2 cells. The particle size and zeta potential of both lipoplexes depended on the charge ratio (Figs. 1, 2). Since the particle size and zeta potential of both lipoplexes were almost identical at the same charge ratio, the effect of galactosylation of the lipoplex on cellular uptake, gene expression, and cytotoxicity could also be compared.

The uptake of galactosylated lipoplex was significantly higher than that of lipoplex, suggesting that the asialoglycoprotein receptor-mediated uptake was efficient by HepG2 cells. To investigate the gene expression characteristics of galactosylated lipoplex in HepG2 cells, the effect of the charge ratio (− : +) on gene expression was measured. Gene expression by galactosylated lipoplex was significantly higher than that by lipoplex at a charge ratio (− : +) of 1.0 : 1.2 to 1.0 : 4.7. These observations supported partially our previous report describing that galactosylated lipoplex was more efficiently taken up by HepG2 cells and/or hepatocytes *via* asialoglycoprotein receptors at a charge ratio (− : +) of 1.0 : 2.3.[8,15] In both lipoplexes, the highest gene expression was observed at a charge ratio (− : +) of 1.0 : 2.3 and transfection efficacy was reduced at higher charge ratios. This observation agrees with the previous reports about conventional lipoplex in various types of cells,[16,17] sterylglucoside-containing lipoplex in HepG2 cells,[18] and mannosylated lipoplex in macrophages by the uptake of mannose receptor.[19]

As shown in Fig. 4, the optimal charge ratio for gene ex-

pression was 1.0 : 2.3. However, the cellular association of plasmid DNA at 4 and 37 °C increased in parallel with the charge ratio of both lipoplexes (Fig. 3). Both lipoplexes bind to the cell surface due to an electrostatic interaction between the positive charges of the cationic liposomes and the negative charges on the cell surface.[11] Therefore, it is likely that the increased zeta potential of the complex at higher charge ratios will result in enhanced DNA cellular association. Taking these factors into consideration, the intracellular trafficking, rather than the degree of uptake of galactosylated lipoplex, is the key process for gene expression.

The cellular association and gene expression of galactosylated lipoplex at a charge ratio of 1.0 : 1.2 were relatively lower than those of other charge ratios and of the lipoplex (Figs. 3, 4). We previously reported that the galactose density of galactosylated liposomes is important for both effective recognition by asialoglycoprotein receptors and cell internalization *in vivo*.[20] Therefore, more galactose might be required on the surface of the lipoplex for efficient recognition by asialoglycoprotein receptors on HepG2 cells. At a charge ratio of 1.0 : 1.2, the transfection activity of galactosylated lipoplex was significantly higher than that of lipoplex although the cellular association was similar. Mammalian cells express several types of lectins involved in intracellular trafficking, including endocytosis, interorganelle routing and putative nuclear transport.[21] Recently, Klink *et al.* reported that lactosylated poly-L-lysine/plasmid DNA complex could localized in the nucleus by targeting a potential lectin-like protein with galactose/lactose specificity.[22] More recently, Wada *et al.* suggested a similar mechanism to explain the high transfection obtained using a galactosylated dendrimer/α-cyclodextrin conjugate.[23] These observations suggest that the transfection activity of galactosylated lipoplex is efficiently transported to the nucleus for efficient gene expression. Further studies are needed to clarify the mechanism governing the efficient nuclear localization by galactosylated lipoplex.

It has been suggested that the inhibition of transfection efficiency at higher charge ratios is most likely due to cytotoxicity in a series of *in vitro* transfection experiments.[1,24] Although there was a slight reduction in the amounts of formazan crystals in the other cells, the lipoplex exhibited no significant toxicity at any charge ratio (Fig. 6). Therefore, cytotoxicity does not play a major role in determining the optimal charge ratio in both forms of lipoplex-mediated transfection performed under our experimental conditions in HepG2 cells.

In conclusion, it is suggested that intracellular trafficking, rather than the degree of uptake and cytotoxicity, is the important process that determines the optimal charge ratio of galactosylated lipoplex in HepG2 cells. The information in this study will be valuable for the future use, design, and development of more efficient galactosylated lipoplexes for hepatocyte-selective gene transfer *via* asialoglycoprotein receptor-mediated endocytosis.

Acknowledgements This work was supported in part by Grants-in-Aid for Scientific Research from Ministry of Education, Culture, Sports, Science, and Technology of Japan, and by Health and Labour Sciences Research Grants for Research on Advanced Medical Technology from the Ministry of Health, Labour and Welfare of Japan.

REFERENCES

1) Felgner P. L., Gadek T. R., Holm M., Roman R., Chan H. W., Wenz M., Northrop J. P., Ringold G. M., Danielsen M., *Proc. Natl. Acad. Sci. U.S.A.*, **84**, 7413—7417 (1987).
2) Liu Y., Liggitt D., Zhong W., Tu G., Gaensler K., Debs R., *J. Biol. Chem.*, **270**, 24864—24870 (1995).
3) Kawakami S., Ito Y., Fumoto S., Yamashita F., Hashida M., *J. Gene Med.*, **7**, 1526—1533 (2005).
4) Li W., Ishida T., Okada Y., Oku N., Kiwada H., *Biol. Pharm. Bull.*, **28**, 701—706 (2005).
5) Wu G. Y., Wu C. H., *J. Biol. Chem.*, **263**, 14621—14624 (1988).
6) Sun X., Hai L., Hu H. Y., Zhang Z. R., *J. Drug Target.*, **13**, 121—128 (2005).
7) Kim T. H., Kim S. I., Akaike T., Cho C. S., *J. Control. Release*, **105**, 354—366 (2005).
8) Kawakami S., Fumoto S., Nishikawa M., Yamashita F., Hashida M., *Pharm. Res.*, **17**, 306—313 (2000).
9) Fumoto S., Kawakami S., Ito Y., Shigeta K., Yamashita F., Hashida M., *Mol. Ther.*, **10**, 719—729 (2004).
10) Fumoto S., Kawakami S., Shigeta K., Higuchi Y., Yamashita F., Hashida M., *J. Pharmacol. Exp. Ther.*, **315**, 484—493 (2005).
11) Sakurai F., Inoue R., Nishino Y., Okuda A., Matsumoto O., Taga T., Yamashita F., Takakura Y., Hashida M., *J. Control. Release*, **66**, 255—269 (2000).
12) Farhood H., Serbina N., Huang L., *Biochim. Biophys. Acta*, **1235**, 289—295 (1995).
13) Kawakami S., Yamashita F., Nishikawa M., Takakura Y., Hashida M., *Biochem. Biophys. Res. Commun.*, **252**, 78—83 (1998).
14) Yang J. P., Huang L., *Gene Ther.*, **5**, 380—387 (1997).
15) Fumoto S., Nakadori F., Kawakami S., Nishikawa M., Yamashita F., Hashida M., *Pharm. Res.*, **20**, 1452—1459 (2003).
16) Felgner J. H., Kumar R., Sridhar C. N., Wheeler C. J., Tsai Y. J., Border R., Ramsey P., Martin M., Felgner P. L., *J. Biol. Chem.*, **269**, 2550—2561 (1994).
17) Yang J. P., Huang L., *Gene Ther.*, **4**, 950—960 (1997).
18) Hwang S. H., Hayashi K., Takayama K., Maitani Y., *Gene Ther.*, **8**, 1276—1280 (2001).
19) Kawakami S., Sato A., Nishikawa M., Yamashita F., Hashida M., *Gene Ther.*, **7**, 292—299 (2000).
20) Managit C., Kawakami S., Yamashita F., Hashida M., *J. Pharm. Sci.*, **94**, 2266—2275 (2005).
21) Monsigny M., Rondanino C., Duverger E., Fajac I., Roche A. C., *Biochim. Biophys. Acta*, **1673**, 94—103 (2004).
22) Klink D. T., Chao S., Glick M. C., Scanlin T. F., *Mol. Ther.*, **3**, 831—841 (2001).
23) Wada K., Arima H., Tsutsumi T., Hirayama F., Uekama K., *Biol. Pharm. Bull.*, **28**, 500—505 (2005).
24) Gao X., Huang L., *Biochem. Biophys. Res. Commun.*, **179**, 280—285 (1991).

Journal of Drug Targeting, September 2006; 14(8): 536–545

informa
healthcare

Basic fibroblast growth factor-binding peptide as a novel targeting ligand of drug carrier to tumor cells

TAKESHI TERADA, MIKI MIZOBATA, SHIGERU KAWAKAMI, YOSHIYUKI YABE, FUMIYOSHI YAMASHITA, & MITSURU HASHIDA

Department of Drug Delivery Research, Graduate School of Pharmaceutical Sciences, Kyoto University, Kyoto 606-8501, Japan

Abstract

Drug systems targeting tumor cells using basic fibroblast growth factor (bFGF) have been widely reported. In this study, the peptide KRTGQYKLC (bFGFp), containing cysteine at the carboxyl termination of the bFGF-derived peptide, was applied as a novel ligand targeting tumor cells. bFGFp was conjugated with bovine serum albumin (BSA) and liposomes. The peptide was shown to inhibit the binding of bFGF to FGF receptor-1 (FGFR1). Interestingly, the binding study using surface plasmon resonance (SPR) assay revealed that the bFGFp–BSA was not bound to FGFR1, but was selectively bound to bFGF. Furthermore, the SPR assay showed that bFGFp–BSA is capable of binding to FGFR1 following the pretreatment with bFGF. The confocal microscopy study indicated that the uptake of bFGFp–BSA by NIH3T3 cells, which highly express FGFRs, was significantly enhanced by pretreatment with bFGF. Then, PEGylated liposomes containing bFGFp (bFGFp–liposome) were prepared by conjugating maleimide-PEG-PE with bFGFp. Following the pretreatment of bFGF, the uptake of bFGFp–liposomes by NIH3T3 cells was significantly enhanced. These results suggest that bFGFp–BSA and bFGFp–liposomes are taken by NIH3T3 cells via binding with bFGF. In addition, both bFGFp–BSA and bFGFp–liposomes had no effect on the proliferation of NIH3T3 cells. This strategy can be used as a novel system for targeting tumors highly expressing FGFRs without a proliferation effect.

Keywords: *Basic fibroblast growth factor, targeting, liposome, surface plasmon resonance assay*

Introduction

Basic fibroblast growth factor (bFGF) is a multifunctional protein which has mitogenic, chemotactic and angiogenic activities (Lappi 1995; Compagni et al. 2000). Several recent reports have demonstrated an autocrine role for bFGF in tumor cells (Halaban et al. 1987; Halaban et al. 1988; Dow and deVerre White 2000). Therefore, bFGF and their receptors (FGFRs) are especially produced by a variety of tumor cells and lead to tumor angiogenesis and progression (Klagsbrun et al. 1986; Takanami et al. 1996; Volm et al. 1997). It has recently been reported that the overexpression of FGFRs in tumor cells can be used to achieve successful drug targeting. Targeting of FGFRs by toxin-conjugated or fused bFGF–saporin (a ribosome-inactivating protein) could control the proliferation of tumor cells that highly express FGFRs (Beitz et al. 1992; Ying et al. 1994; Davol and Frackelton 1999). In addition, bFGF retargeted adenovirus (Hoganson et al. 2001; Kleeff et al. 2002; Qin et al. 2005) and the conjugated polylysine with bFGF (Sosnowski et al. 1996; Hoganson et al. 1998) have exhibited high expression in tumor cells with up-regulated FGFRs.

However, bFGF itself is potent inducer of angiogenesis. Although the cell-surface receptors on tumor cells possess intrinsic tyrosine kinase activity and are phosphorylated upon binding of bFGF (Burgess and Maciag 1989; Klagsbrun 1989), bFGF is able to stimulate tumor proliferation, migration and differentiation and/or to induce angiogenesis. Recently, it was reported that bFGF infusion resulted in significant increases in tumor vascularity, blood flow and growth (Gross et al. 1993; Davies et al. 2002). Therefore, since a drug delivery system using

Correspondence: M. Hashida, Department of Drug Delivery Research, Graduate School of Pharmaceutical Sciences, Kyoto University, Kyoto 606-8501, Japan. Tel: 81 75 753 4525. Fax: 81 75 753 4575. E-mail: hashidam@pharm.kyoto-u.ac.jp

ISSN 1061-186X print/ISSN 1029-2330 online © 2006 Informa UK Ltd.
DOI: 10.1080/10611860600849498

bFGF as the targeting ligand can induce proliferation of tumor cells that up-regulate FGFR, a targeting ligand without any proliferation effect is needed.

Recently, Yayon et al. (1993) identified bFGF-derived peptide KRTGQYKL (residues 119–126 of bFGF) as inhibitor of the binding between bFGF and its receptor following examination of a random phage-epitope library. Furthermore, this peptide itself had no tumor proliferation effects and inhibited the proliferation of bovine aortic endothelial cells in complete growth medium.

In this study, bFGF-derived peptide KRTGQYKL was conjugated with bovine serum albumin (BSA) and its cellular binding characteristics were investigated. Sulfo-succinimidyl-4-(*N*-maleidomethyl) cyclohexane-1-carboxylate (sulfo-SMCC), which is a general reagent for connection via surface amino residues to the other molecules with thiolated moieties, was used as a linker between the peptide and BSA. To obtain the conjugate with BSA, we prepared KRTGQYKLC (bFGFp) containing cysteine at the carboxyl terminal and conjugated bFGFp with BSA via the surface amino residues. Surface plasmon resonance (SPR) spectroscopy, which allows real-time detection of macromolecular interactions without using radioactive or fluorescent labeled ligands, was used for this study to confirm the binding of bFGFp–BSA. In addition, we prepared bFGFp–liposomes containing conjugated maleimide-PEG-PE with the peptide and evaluated this strategy, since liposomes have been widely investigated as drug delivery systems (Hashida et al. 2005).

Here, we demonstrate the characteristics of bFGFp–BSA and bFGFp–liposomes as a drug delivery system by an *in vitro* study using NIH3T3 and FGFRs-deficient Chinese hamster ovary (CHO-K1) cells (Rusnati et al. 2002). Interestingly, bFGFp–BSA exhibited high binding to bFGF, but not FGFR1. As far as the uptake characteristics are concerned, bFGFp–BSA exhibited a higher uptake via bFGF in NIH3T3 cells, which express a considerable amount of FGFRs. Based on these findings, we developed novel bFGFp-modified liposomes for tumor-selective drug delivery. In the presence of bFGF, bFGFp-modified liposomes exhibit a higher uptake via bFGF in NIH3T3 cells. Since bFGFp itself has no tumor proliferation effects, bFGFp is an effective potential targeting ligand for targeted delivery to tumor cells.

Materials and methods

Materials

Sulfo-SMCC was purchased from Pierce Biotechnology Inc. (Rockford, IL, USA). Recombinant human bFGF was obtained from PeproTech EC. (London, UK). Recombinant human FGFR1α(IIIc)/Fc chimera was purchased from Techne Co. (Minneapolis, MN, USA). Distearoyl phosphatidylcholine (DSPC), cholesteryl chloroformate and 3-(4,5-dimethylthiazol-2-yl)-2,5-diphenyltetrazolium bromide (MTT) were purchased from Sigma-Aldrich Co. (St Louis, MO, USA). Cholesterol (Chol) and Clear-Sol I were obtained from Nacalai Tesque Inc. (Kyoto, Japan) and Soluene 350 was purchased from Packard Bioscience Co. (Groningen, Netherlands). [^{3}H] CHE was purchased from NEN Life Science Products Inc. (Boston, MA, USA). The peptide KRTGQYKLC (bFGFp) was custom-made by Toray Research Center Inc. (Tokyo, Japan). mPEG$_{3000}$-DSPE was purchased from Avanti Polar Lipids Inc. (Alabama, AL, USA) and Maleimide-PEG$_{2000}$-DSPE was purchased from NOF Co. Inc. (Tokyo, Japan). Dulbecco's-modified Eagle's minimum essential medium (DMEM) and Hank's buffered salt solution (HBSS) were obtained from Nissui Pharmaceutical Co. Ltd. (Tokyo, Japan). Fetal bovine serum (FBS) was obtained from Biowhittaker Co. (Walkersville, MD). All other chemicals were reagent grade products obtained commercially.

Synthesis of bFGFp–BSA

bFGFp–BSA was synthesized according to the method reported previously (Backstrom and Sander-Bush 1997). bFGFp containing cysteine at the carboxyl terminal of bFGF-derived peptide KRTGQYKL was prepared for this synthesis. The SMCC derivatives of BSA were obtained by simultaneous addition of 20 mg BSA and 2.5 mg sulfo-SMCC to 2.0 ml 0.05 M carbonate buffer at pH 8.5 while stirring. After 1 h at room temperature, the mixture was centrifuged by VIVA SPIN 10 kDa cut-off (VIVASCIENCE, Hannover, Germany) to remove any unreacted sulfo-SMCC and then the buffer was changed to distilled water and the solution was lyophilized. Subsequently, 10 mg of the synthetic SMCC–BSA was incubated with 2.0 mg bFGFp in PBS (1.0 ml). After 3 h at 4°C, the mixture was centrifuged by VIVA SPIN to remove unreacted peptide, followed by dialysis and lyophilization. The number of conjugated SMCC and peptide groups was calculated from the number of free amino acid groups determined by trinitrobenzene sulfonic acid using BSA as a standard (Habeeb 1966). Furthermore, the 10 mM L-cysteine solution and the product were mixed at room temperature for 1 h to remove the free maleimide, followed by dialysis and lyophilization.

Synthesis of bFGFp–PEG-DSPE

bFGFp (28 mg, 26 μmol) was dissolved in 0.1 M HEPES buffer (pH 7.0, 2 ml). Maleimide-PEG$_{2000}$-DSPE (50 mg, 17 μmol) and methanol (0.2 ml) were added to the bFGFp solution at 4 °C while stirring.

The reaction was continued at 4°C for 2 days. The mixed solution was dialyzed against distilled water and lyophilized. TLC analysis and ninhydrin assay showed the disappearance of free maleimide-PEG_{2000}-DSPE and the appearance of bFGFp–PEG-DSPE, which indicates that the reaction had gone to completion. The purity of the synthetic bFGFp–PEG-DSPE was determined by fluorescamine assay (Bohlen et al. 1973) and found to be over 90% on the basis of the amino acid content of bFGFp. Furthermore, 10 mM L-cysteine solution and the product were mixed at room temperature for 1 h to remove the free maleimide-PEG_{2000}-DSPE, followed by dialysis and lyophilization.

Preparation of liposomes

Liposomes were prepared by our previously reported method (Kawakami et al. 2000; Kawakami et al. 2001; Managit et al. 2005a). Each lipid mixture (DSPC, Chol, and $mPEG_{3000}$-DSPE) and [^{3}H] CHE were dissolved in chloroform and evaporated to dryness. bFGFp–PEG-DSPE was solved in mixed organic solvent (chloroform: methanol = 1:1) beforehand. The dried lipid films were hydrated in HBSS, sonicated at 65°C for 3 min and then extruded through polycarbonate filters with a pore size of 0.2 μm. Mean particle diameters were determined by laser light scattering using a Zetasizer Nano ZS (Malvern Instruments, Malvern, UK). All liposomes were similar in size (an average diameter of approximately 100 nm) as shown in Table I.

SPR spectroscopy assay

SPR measurements were performed using a BIAcore X (BIAcore, Uppsala, Sweden). bFGFp–BSA or FGFR1 was immobilized on the surface of a CM5 sensor chip using the standard amine coupling procedure of the manufacturer. Briefly, the surface of the chip consisting of flow cells 1 and 2 was activated by exposing them to a mixture of 0.05 M *N*-hydroxysuccinimide (NHS) and 0.2 M *N*-ethyl-*N'*-dimethyl aminopropyl carbodiimide (EDC) for 7 min. Flow cell 1 was immobilized with bFGFp–BSA or FGFR1 in acetate buffer (pH 4.0). The immobilized amount of bFGFp–BSA and FGFR1 were approximately 8000 and 5000 resonance units (RU), respectively. Flow cell 2 was immobilized using the same amount as for flow cell 1 by BSA to be used as a blank sensorgram for subtraction of the bulk refractive index background. Finally, the unreacted sites of both immobilized flow cell were blocked with 0.1 M ethanolamine (pH 8.5). All reagents were injected at a flow rate of 5.0 μl/min.

Each sample was adjusted to an appropriate concentration using a running buffer (150 mM NaCl, 10 mM HEPES, pH 7.4). The mixed solution of bFGF and bFGFp or bFGF and bFGFp–BSA was prepared 30 min before the SPR study. In all studies, each sample was allowed to flow at a rate of 10 μl/min at 25°C for 2 min and dissociated for 2 min. The regeneration of the sensor chip was carried out by injection of 10 μl 50 mM HCl.

The sensorgram was analyzed by a global fitting procedure using a 1:1 (Langmuir-type) binding model-derived equation that is available in the BIAevaluation 3.0 software. The dissociation constant (K_d) was determined from k_d/k_a.

Table I. Lipid composition and mean particle size of liposomes investigated.

Lipid composition (molar ratio)	Particle size (nm)
DSPE/Chol/bFGFp–PEG-DSPE (60:30:10)	93 ± 2.21
DSPE/Chol/bFGFp–PEG-DSPE (60:35:5)	115 ± 7.61
DSPE/Chol/bFGFp–PEG-DSPE (60:37.5:2.5)	100 ± 1.76
DSPE/Chol/bFGFp–PEG-DSPE (60:39:1)	114 ± 1.99
DSPE/Chol/mPEG-DSPE (60:39:1)	101 ± 1.71

Results are expressed as the means ± SD of three experiments.

Cellular association and visualization of FITC labeled bFGFp–BSA and BSA

SMCC–BSA and bFGFp–Cys–SMCC–BSA were labeled with FITC as previously described (Monsigny et al. 1984). Briefly, BSA before the modification of SMCC was incubated with three equivalents of FITC in 0.1 M sodium carbonate buffer, pH 9.5 solution by stirring for 5 h at room temperature. The mixture was centrifuged by VIVA SPIN to remove the unreacted FITC and then purified by dialysis with distilled water and lyophilized. The FITC–BSA was used for the modification of bFGFp as described above.

NIH3T3 cells were seeded on glass coverslips in 12-well plates at a density of 1×10^5 cells/well. After complete adhesion, the cells were washed 3-times with HBSS and incubated at 37°C for 2 h with each FITC-labeled protein (50 μg/ml) dissolved in HBSS. After incubation, the protein solution was removed and the cells were washed 3-times with HBSS, then fixed with 4% paraformaldehyde in PBS and incubated at room temperature for over 20 min. After washing twice with PBS, they were treated with 0.2% Triton X-100–PBS, 5 μg/ml RNase A and 0.5 μg/ml propidium iodide in 0.1 M Tris–HCl (pH 7.4) containing 0.1 M NaCl for nuclei staining. Then, they were mounted in glycerol:PBS (1:1) containing 2.5% 1,4-diazobicyclo (2,2,2) octane. Images were then obtained by confocal laser scanning microscopy (MRC-1024, Bio-Rad, Hercules, CA, USA).

Cellular association experiments with [^{3}H] CHE labeled bFGFp–liposomes

A cellular association study was performed using our previously reported method (Opanasopit et al. 2001; Managit et al. 2005b). Briefly, NIH3T3 and CHO-K1 cells were plated on 12-well culture plates at a density of 1×10^5 cells/well. After 24 h cultivation, the cells were washed 3-times with HBSS and incubated with each lot of treated [^{3}H] CHE labeled liposomes (100 μM) in HBSS at 37°C. The pretreatment of each lot of liposomes by bFGF was carried out 30 min before the uptake study. After 2 h of incubation, the medium was removed and the cells were washed 5-times with HBSS. The cells were then solubilized with 0.5 ml 1.0 N NaOH solution overnight and then neutralized with 0.1 ml 5.0 N HCl solution. The radioactivity was measured in a scintillation counter (LSA-500, Beckman, Tokyo, Japan). The amount of cellular protein in each cell lysate was estimated using a protein quantification kit (Dojindo Molecular Technologies, Inc. Gaithersburg, MD, USA).

Cell proliferation assay

The effect on cell proliferation produced by bFGFp–BSA and –liposomes in presence or absence of bFGF was assessed by MTT assay (Mosmann 1983). Briefly, NIH3T3 cells were counted and seeded in 96-well plates at a density of 4×10^3 cells/well. After 24 h of incubation, the cells were exposed to samples diluted in DMEM without FBS. After 72 h of incubation, MTT assay was performed in triplicate.

Statistical analysis

Statistical comparisons were performed by Student's *t*-test for two groups. $P < 0.05$ was considered to be indicative of statistical significance.

Results

The interaction analysis of bFGFp–BSA with FGFR1 and bFGF

To clarify the characterization of the binding of bFGF-derived peptide KRTGQYKL with FGFR1 and bFGF, bFGFp containing cysteine at the carboxyl terminal of the peptide sequence was conjugated with BSA using sulfo-SMCC and the interaction was evaluated by SPR spectroscopy. The amount of incorporated bFGFp calculated from the amino acid groups was about 12 peptides per molecule of BSA.

The conjugated bFGFp–BSA was immobilized on the surface of a sensor chip CM5 by amine coupling. Non-specific binding of an analyte and any change in bulk refractive index were ruled out by immobilizing BSA as a control. Although the bFGFp-containing peptide sequence was reported to inhibit the interaction between bFGF and FGFR1 (Yayon et al. 1993), no response signal was observed in FGFR1 (Figure 1(A)). However, bFGF exhibited a significantly high response signal and this response of bFGF was reduced in the presence of bFGFp. The binding of bFGF to bFGFp–BSA was completely regenerated by the injection of 50 mM HCl (Figure 1(B)), suggesting that the interaction does not involve chemical binding via any active groups. These results suggest that bFGFp–BSA does not bind to FGFR1, but binds to bFGF. The injected bFGF bound to bFGFp–BSA in a concentration-dependent manner and the dissociation was very slow, indicating that the binding affinity was high (Figure 1(C)). The association and

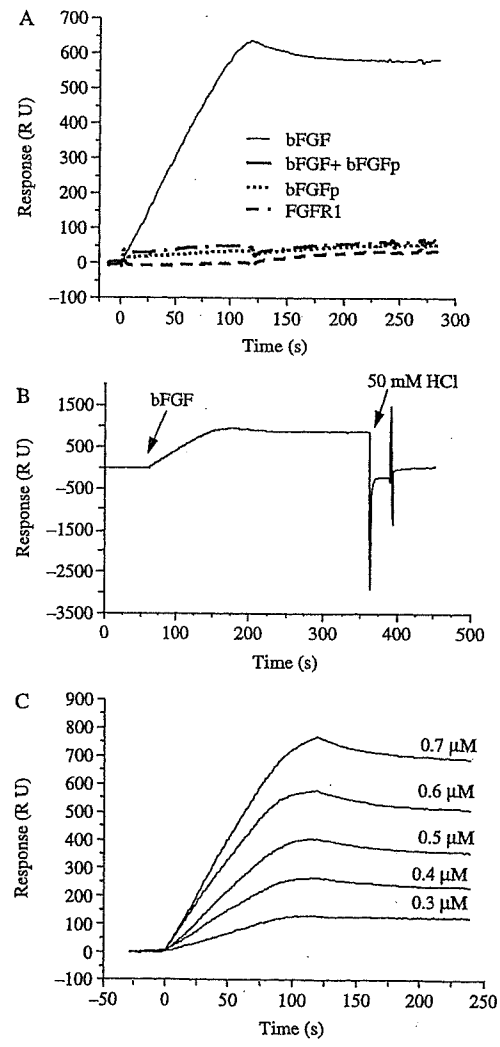

Figure 1. SPR sensorgrams of bFGF binding to bFGFp–BSA. (A) 10 μg/ml bFGF, the mixture of 10 μg/ml bFGF and 100 μg/ml bFGFp, 100 μg/ml bFGFp and 10 μg/ml FGFR1 were injected over immobilized bFGFp–BSA. (B) 10 μg/ml bFGF was injected onto the sensor chip. Subsequently, the sensor chip was completely regenerated by the injection 50 mM HCl. (C) Different concentrations of bFGF were injected over immobilized bFGFp–BSA. Each sensorgram was overlaid and zeroed on the *y*-axis to the average baseline. The start injection time for each sample was set to zero on the *x*-axis.

Table II. Rate constants and dissociation constants for the interaction between immobilized bFGFp–BSA and bFGF.

	Rate constants		Dissociation constant
	$k_a \times 10^{-3}$ ($M^{-1}s^{-1}$)	$k_d \times 10^{4}$ (s^{-1})	$K_d \times 10^{8}$ (M)
bFGF	4.09 ± 0.727	4.83 ± 0.857	12.2 ± 3.52

Results are expressed as the means ± SD of three replicates.

dissociation rate constants were estimated by global fitting to sensorgrams using a 1:1 (Langmuir-type) binding model-derived equation. The calculated dissociation constant was $12.2 \pm 3.52 \times 10^{-8}$ M (Table II).

The binding of bFGFp–BSA to FGFR1 via bFGF

FGFR1 and BSA as a control were immobilized on the surface of a sensor chip CM5 by amine coupling as described above. Although bFGF showed a significantly high response signal (Figure 2), no response signal was observed with bFGFp–BSA, suggesting that bFGFp–BSA does not bind to FGFR1. In addition, the response signal of bFGFp–BSA pre-incubated with bFGF was much higher than that of bFGF itself, suggesting that bFGFp–BSA pre-incubated with bFGF is capable of binding to FGFR1 via bFGF.

The effect of bFGF on the uptake of bFGFp –BSA by NIH3T3 cells

The uptake of bFGFp–BSA by NIH3T3 cells, overexpressing FGFRs, was evaluated by confocal microscopy. FITC-labeled BSA or bFGFp–BSA was incubated with the cells in presence of bFGF or the mixture of bFGF with an excess of bFGFp. The uptake of bFGFp–BSA pre-incubated with bFGF was significantly higher than that of bFGF–BSA alone (Figure 3). However, in the case of BSA, there was no difference when bFGF was present or not. The higher uptake was significantly reduced by the mixture of bFGF with an excess of bFGFp, suggesting that the increase in fluorescence in the cells of bFGFp–BSA pre-incubated with bFGF was due to the FGFR-mediated endocytosis.

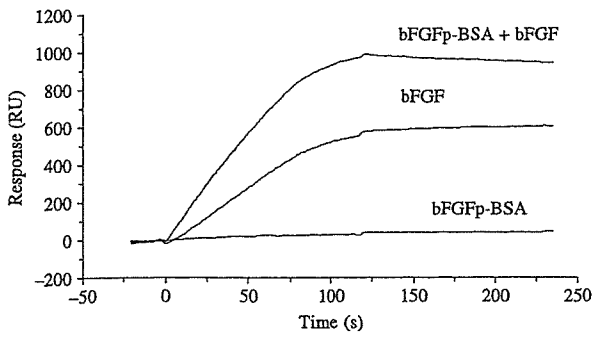

Figure 2. SPR sensorgram of binding of bFGFp–BSA to FGFR1 via bFGF. About 100 μg/ml bFGFp–BSA, 5 μg/ml bFGF and the mixture of 100 μg/ml bFGFp–BSA and 5 μg/ml bFGF were injected over the immobilized FGFR1.

The effect of bFGF on the uptake of bFGFp–liposomes by NIH3T3 cells

To further evaluate this strategy using bFGFp-conjugated delivery systems, we prepared liposomes containing different amounts of bFGFp–PEG_{2000}-DSPE conjugated maleimide-PEG-DSPE with bFGFp as a novel tumor-selective liposome. Table I summarizes the lipid composition and particle size of the liposomes prepared. All filtered liposomes were similar in size (average diameter approximately 100 nm). All pretreated bFGFp–liposomes with bFGF exhibited a higher uptake than the untreated group (Figure 4). In particular, in the condition with 1 μg/ml bFGF, 2.5 and 5.0% bFGFp–liposomes exhibited a high effect of bFGF in comparison with 1.0 and 10%. Furthermore, similar to bFGFp–BSA, bFGFp–liposomes tended to exhibit a high uptake even without the addition of bFGF, though the uptake was less than that of bFGFp–liposome with bFGF, and this was dependent on the amount of bFGFp–PEG_{2000}-DSPE. It suggests that bFGFp–liposome might indicate the cellular uptake not only by the interaction with FGFRs via binding to bFGF but also by the other cause.

The effect of bFGF on the uptake of bFGFp–liposomes by CHO-K1 cells

To determine whether the high uptake in NIH3T3 cells by the addition of bFGF is via FGFRs, the uptake study was also conducted using FGFRs-deficient CHO-K1 cells. The addition of bFGF did not enhance the uptake of 5.0 and 10% bFGFp–liposomes, but inhibited it (Figure 5(A)). In addition, the inhibition was dependent on the concentration of the added bFGF (Figure 5(B)). These results support the hypothesis that bFGFp–liposomes are capable of binding to bFGF and the effect of bFGF in NIH3T3 cells may be due to the uptake via FGFRs.

The effect of bFGFp-conjugated delivery systems on the viability and proliferation of NIH3T3 cells

bFGF is known to exhibit a strong proliferative effect on most tumor cells. To determine the effect of bFGFp-conjugated delivery systems on the viability and proliferation of tumor cells, NIH3T3 cells were incubated with bFGFp, bFGFp–BSA, and bFGFp–liposomes in the absence or presence of 1 nM bFGF (Figure 6(A),(B)). In this study, 0.72 and

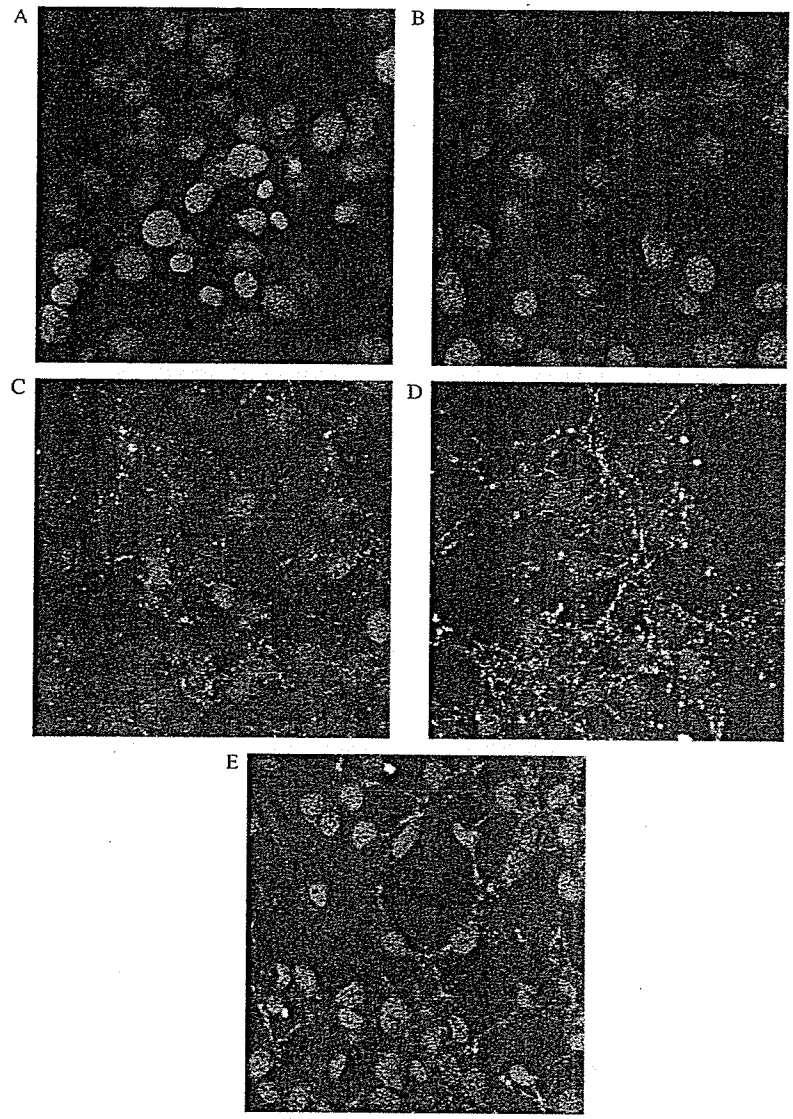

Figure 3. Confocal microscopy of FITC–BSA and FITC–bFGFp–BSA preincubated with bFGF in NIH3T3 cells. NIH3T3 cells were incubated with FITC–BSA (A), a mixture of FITC–BSA and bFGF (B), FITC–bFGFp–BSA (C), a mixture of FITC–bFGFp–BSA and bFGF (D), and a mixture of FITC–bFGFp–BSA, bFGF and bFGFp (E) at 37°C for 2 h. Red signals indicate the nuclei stained with propidium iodide.

7.2 μg/ml bFGFp–BSA and 4.0 and 40 μM bFGFp–liposomes contained 0.1 and 1.0 μM of conjugated bFGFp, respectively. The incubation with an excess of bFGFp, bFGFp–BSA and bFGFp–liposomes had no cell proliferation of cells in the absence of bFGF. Furthermore, in the presence of bFGF, the incubation had no influence on the proliferation by bFGF, although bFGFp is capable of binding to bFGF.

Discussion

The bFGF-derived peptide KRTGQYKL (residues 119–126 of bFGF) has been reported to inhibit the binding of bFGF to FGFR1 (Yayon et al. 1993) and to have no cell proliferation effect. Since FGFRs are overexpressed on the surface of many tumor cells, we hypothesized that the conjugated peptide carrier would be capable of delivering antitumor drugs to tumor cells via direct binding to FGFRs, without inducing any tumor growth.

To examine the binding ability, we firstly prepared bFGFp–BSA-conjugated BSA to the peptide using sulfo-SMCC and evaluated this compound using SPR spectroscopy, which has been widely used as a tool to study biomolecular interactions including those between receptors and ligands (Wu and Chaiken 2004), DNA–protein (Wegner et al. 2003; Schubert et al. 2003) and protein–protein interactions (Stenlund et al. 2003). Although FGFR1 exhibited no binding to the immobilized bFGFp–BSA, bFGF showed a specific interaction via the presence of bFGFp on the surface of BSA (Figure 1). Although these results were different from our hypothesis, the

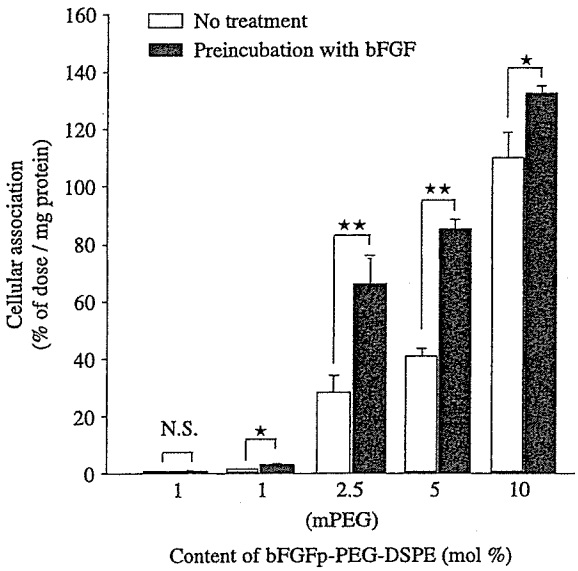

Figure 4. The uptake of [^{3}H]mPEG-liposomes and [^{3}H]bFGFp–liposomes containing different amounts of bFGFp–PEG-DSPE (100 μM) with (■) and without 1 μg/ml bFGF (□) for 2 h by NIH3T3 cells. Results are expressed as the mean ± SD values ($n = 3$). Statistical analysis was performed by Student's t-test (**, $P < 0.01$; *, $P < 0.05$; NS, not significant).

interaction between bFGF-derived peptide and bFGF could be explained by the oligomeric self-association of bFGF (Venkataraman et al. 1996; Davis et al. 1999). Safran et al. (2000) showed that the essential residues of bFGF allow inter-monomer interactions that stabilize the bFGF dimer. The used peptide (KRTGQYKL) in this study is included in the sequence contributing to the construction of the bFGF dimer or oligomer. Taking these facts into consideration, the peptide may bind to bFGF via the sequence involved in bFGF self-association.

As shown in Figure 2, we found that bFGFp–BSA binds to FGFR1 via bFGF and this result suggests that the binding site of bFGF to bFGFp–BSA is different from that of FGFR1. This observation agrees with the report by Davis et al. (1999) who found that there are separate sites for bFGF self-association and receptor binding on the surface of bFGF. Therefore, it suggests that the binding bFGF to bFGFp–BSA would inhibit the intact interaction between the bFGF and FGFR1. Tumor cells, such as melanoma, breast cancer and prostate cancer, are reported to exhibit overexpression of bFGF and FGFRs (Penault-Llorca et al. 1995; Danielsen and Rofstad 1998; Kwabi-Addo et al. 2004). Furthermore, such tumor tissues possess high concentrations of bFGF (Giri et al 1999). Furthermore, the low dissociation constant of the interaction between bFGFp–BSA and bFGF suggests the possibility of a novel targeting strategy (Table II). Therefore, our observations suggest that the conjugated peptide carrier would be capable of delivering antitumor drugs to tumor cells with FGFRs via binding to bFGF.

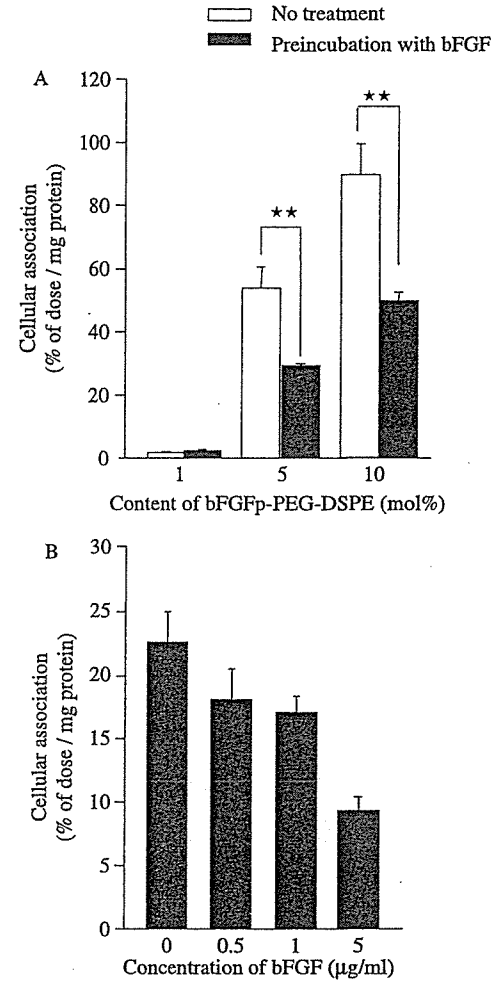

Figure 5. The uptake of [^{3}H]bFGFp–liposomes with (■) and without 1 μg/ml bFGF (□) for 2 h by CHO-K1 cells. (A) The effect of the amount of bFGFp–PEG-DSPE contained in bFGFp–liposomes was investigated. (B) The effect of the concentration of bFGF preincubated with 2.5% bFGFp–liposome was investigated. Results are expressed as the mean ± SD values ($n = 3$). Statistical analysis was performed by Student's t-test (**, $P < 0.01$).

The receptor-mediated internalization allows the liposomes to avoid the action of multi drug resistant (MDR) transporters like *P*-glycoprotein (Sapra and Allen 2003). Therefore, the internalization of drug carrier in the tumor cells allows an enhancement of the pharmacological effects of the antitumor drug. Some groups have reported that bFGF binding to FGFRs is internalized and translated to the nucleus, subsequently inducing cell proliferation (Baldin et al. 1990; Olsnes et al. 2003; Soulet et al. 2005). Our confocal microscopy study revealed that bFGF enhances the internalization of bFGFp–BSA (Figure 3). In contrast, this effect was not observed in the case of BSA. Furthermore, pretreatment by the mixture of bFGFp and bFGF did not enhance the internalization via exogenous bFGF. These results provide evidence that the increase in the internalization by bFGF is due to the binding of bFGFp–BSA

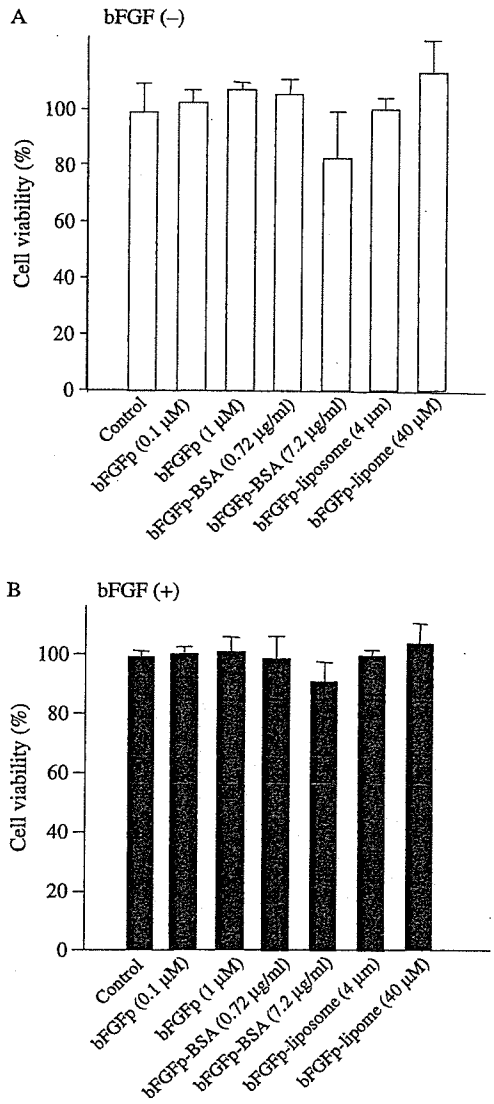

Figure 6. Effects of bFGFp and the drug delivery system using bFGFp on the cell viability of NIH3T3 cells without (A) and with (B) 1 nM bFGF. Each bFGFp and drug delivery system, following adjustment to the appropriate concentration, were added to NIH3T3 cells. After 72 h, the cell viability was investigated by MTT assay. Each value represents the mean ± SD values ($n = 3$).

to FGFRs expressed by NIH3T3 cells via bFGF and not due to the physiological effect of bFGF itself.

Liposomes have been widely investigated as drug delivery carriers. The modification by targeting ligand to the PEG terminal results in PEG-liposomes exhibiting both prolonged circulation and effective target binding. Therefore, bFGFp–liposomes with bFGFp on the PEG terminus were prepared and evaluated as a novel ligand to target tumor cells. Following the addition of bFGF, the uptake of liposomes containing different amounts of bFGFp–PEG-DSPE by NIH3T3 cells was enhanced similar to bFGFp–BSA (Figure 4). In particular, bFGFp–liposomes containing 2.5 and 5.0% bFGFp–PEG-DSPE exhibited and increased uptake following the addition of bFGF. However, the increase in the uptake of PEG-liposomes following the addition of bFGF was barely detectable, indicating that the binding of the peptide in bFGFp–liposomes to bFGF is essential for enhanced uptake.

In order to investigate whether bFGFp–liposomes bound to bFGF are taken up via FGFRs in NIH3T3 cells, the uptake using CHO-K1 cells, deficient in FGFRs (Rusnati et al. 2002), was examined. Unlike the case of NIH3T3 cells, pretreatment by bFGF resulted in no increase in uptake, rather a reduction in CHO-K1 cells (Figure 5). Furthermore, the uptake decreased according to the concentration of bFGF used for pretreatment. These results suggest that the unexpected uptake of bFGFp–liposomes in CHO-K1 cells is inhibited by binding to bFGF. These observations suggest that the increased uptake by NIH3T3 cells is due to uptake via FGFRs.

Although bFGF enhanced the proliferation effect of NIH3T3 cells overexpressing FGFRs, incubation with an excess of bFGFp–BSA, bFGFp–liposome and bFGFp alone produced no proliferation effect (Figure 6(A)). Therefore, it is expected that bFGFp–liposomes do not induce tumor cell proliferation. In addition, regardless of the binding of bFGF to conjugated carriers by bFGFp, bFGF in the presence of an excess of conjugated carriers exhibits the same proliferation effect as bFGF alone (Figure 6(B)). The result shows that the binding to bFGFp–liposomes has no effect on the proliferation produced by bFGF and supports the view that bFGFp–liposome binding to bFGF might be recognized by FGFRs.

In all studies, an unexpected uptake without the addition of bFGF was observed. bFGFp–liposomes exhibited unexpected uptake in NIH3T3 and CHO-K1 cells and the effect increased according to the amount of bFGFp–PEG-DSPE. One possible explanation of this is that the cationic nature of bFGFp might induce unexpected binding to the cells. Another explanation is that bFGFp might bind to any receptor on the surface of the cells. The screening of functional peptides without unexpected binding may allow the successful application of this strategy. Alternatively, the incorporation into bFGFp–liposomes of PE-PEG with a short enough length to reduce the unexpected binding may enhance the targeting efficiency to FGFRs via bFGF. Immunoliposomes incorporating PE-PEG have been reported to prolong blood circulation in the body (Maruyama 2002).

In summary, the current studies demonstrated that bFGFp is capable of binding to bFGF and the bFGFp/bFGF is able to bind to FGFR. Furthermore, the drug delivery system using bFGFp was taken up in the cells overexpressing FGFRs via binding to bFGF. Although some problems still need to be overcome, this finding provides new information to help in the development of safe and effective drug delivery system targeting tumor cells.

Acknowledgements

This work was partly supported by Grant-in-Acids for Scientific Research and 21st Century COE Program "Knowledge Information Infrastructure for Genome Science" from the Ministry of Education, Culture, Sports, Science and Technology, Japan.

References

Backstrom JR, Sanders-Bush E. 1997. Generation of anti-peptide antibodies against serotonin 5-HT2A and 5-HT2C receptors. J Neurosci Methods 77:109–117.

Baldin V, Roman AM, Bosc-Bierne I, Amalric F, Bouche G. 1990. Translocation of bFGF to the nucleus is G1 phase cell cycle specific in bovine aortic endothelial cells. EMBO J 9:1511–1517.

Beitz JG, Davol P, Clark JW, Kato J, Medina M, Frackelton AR, Jr, Lappi DA, Baird A, Calabresi P. 1992. Antitumor activity of basic fibroblast growth factor–saporin mitotoxin *in vitro* and *in vivo*. Cancer Res 52:227–230.

Bohlen P, Stein S, Dairman W, Udenfriend S. 1973. Fluorometric assay of proteins in the nanogram range. Arch Biochem Biophys 155:213–220.

Burgess WH, Maciag T. 1989. The heparin-binding (fibroblast) growth factor family of proteins. Annu Rev Biochem 58:575–606.

Compagni A, Wilgenbus P, Impagnatiello MA, Cotten M, Christofori G. 2000. Fibroblast growth factors are required for efficient tumor angiogenesis. Cancer Res 60:7163–7169.

Danielsen T, Rofstad EK. 1998. VEGF, bFGF and EGF in the angiogenesis of human melanoma xenografts. Int J Cancer 76:836–841.

Davies MM, Burke D, Carnochan P, Glover C, Kaur S, Allen-Mersh TG. 2002. Basic fibroblast growth factor infusion increases tumour vascularity, blood flow and chemotherapy uptake. Acta Oncol 41:84–90.

Davis JC, Venkataraman G, Shriver Z, Raj PA, Sasisekharan R. 1999. Oligomeric self-association of basic fibroblast growth factor in the absence of heparin-like glycosaminoglycans. Biochem J 341:613–620.

Davol PA, Frackelton AR, Jr. 1999. Targeting human prostatic carcinoma through basic fibroblast growth factor receptors in an animal model: Characterizing and circumventing mechanisms of tumor resistance. Prostate 40:178–191.

Dow JK, deVere White RW. 2000. Fibroblast growth factor 2: Its structure and property, paracrine function, tumor angiogenesis, and prostate-related mitogenic and oncogenic functions. Urology 55:800–806.

Giri D, Ropiquet F, Ittmann M. 1999. Alterations in expression of basic fibroblast growth factor (FGF) 2 and its receptor FGFR-1 in human prostate cancer. Clin Cancer Res 5:1063–1071.

Gross JL, Herblin WF, Dusak BA, Czerniak P, Diamond MD, Sun T, Eidsvoog K, Dexter DL, Yayon A. 1993. Effects of modulation of basic fibroblast growth factor on tumor growth *in vivo*. J Natl Cancer Inst 85:121–131.

Habeeb AF. 1966. Determination of free amino groups in proteins by trinitrobenzenesulfonic acid. Anal Biochem 14:328–336.

Halaban R, Ghosh S, Baird A. 1987. bFGF is the putative natural growth factor for human melanocytes. *In Vitro* Cell Dev Biol 23:47–52.

Halaban R, Kwon BS, Ghosh S, Delli Bovi P, Baird A. 1988. bFGF as an autocrine growth factor for human melanomas. Oncogene Res 3:177–186.

Hashida M, Kawakami S, Yamashita F. 2005. Lipid carrier systems for targeted drug and gene delivery. Chem Pharm Bull 53:871–880.

Hoganson DK, Chandler LA, Fleurbaaij GA, Ying W, Black ME, Doukas J, Pierce GF, Baird A, Sosnowski BA. 1998. Targeted delivery of DNA encoding cytotoxic proteins through high-affinity fibroblast growth factor receptors. Hum Gene Ther 9:2565–2575.

Hoganson DK, Sosnowski BA, Pierce GF, Doukas J. 2001. Uptake of adenoviral vectors via fibroblast growth factor receptors involves intracellular pathways that differ from the targeting ligand. Mol Ther 3:105–112.

Kawakami S, Wong J, Sato A, Hattori Y, Yamashita F, Hashida M. 2000. Biodistribution characteristics of mannosylated, fucosylated, and galactosylated liposomes in mice. Biochim Biophys Acta 1524:258–265.

Kawakami S, Munakata C, Fumoto S, Yamashita F, Hashida M. 2001. Novel galactosylated liposomes for hepatocyte-selective targeting of lipophilic drugs. J Pharm Sci 90:105–113.

Klagsbrun M, Sasse J, Sullivan R, Smith JA. 1986. Human tumor cells synthesize an endothelial cell growth factor that is structurally related to basic fibroblast growth factor. Proc Natl Acad Sci USA 83:2448–2452.

Klagsbrun M. 1989. The fibroblast growth factor family: Structural and biological properties. Prog Growth Factor Res 1:207–235.

Kleeff J, Fukahi K, Lopez ME, Friess H, Buchler MW, Sosnowski BA, Korc M. 2002. Targeting of suicide gene delivery in pancreatic cancer cells via FGF receptors. Cancer Gene Ther 9:522–532.

Kwabi-Addo B, Ozen M, Ittmann M. 2004. The role of fibroblast growth factors and their receptors in prostate cancer. Endocr Relat Cancer 11:709–724.

Lappi DA. 1995. Tumor targeting through fibroblast growth factor receptors. Semin Cancer Biol 6:279–288.

Managit C, Kawakami S, Yamashita F, Hashida M. 2005a. Effect of galactose density on asialoglycoprotein receptor-mediated uptake of galactosylated liposomes. J Pharm Sci 94:2266–2275.

Managit C, Kawakami S, Yamashita F, Hashida M. 2005b. Uptake characteristics of galactosylated emulsion by HepG2 hepatoma cells. Int J Pharm 301:255–261.

Maruyama K. 2002. PEG-immunoliposome. Biosci Rep 22:251–266.

Monsigny M, Roche AC, Midoux P. 1984. Uptake of neoglycoproteins via membrane lectin(s) of L1210 cells evidenced by quantitative flow cytofluorometry and drug targeting. Biol Cell 51:187–196.

Mosmann T. 1983. Rapid colorimetric assay for cellular growth and survival: Application to proliferation and cytotoxicity assays. J Immunol Methods 65:55–63.

Olsnes S, Klingenberg O, Wiedlocha A. 2003. Transport of exogenous growth factors and cytokines to the cytosol and to the nucleus. Physiol Rev 83:163–182.

Opanasopit P, Higuchi Y, Kawakami S, Yamashita F, Nishikawa M, Hashida M. 2001. Involvement of serum mannan binding proteins and mannose reseptors in uptake of mannosylated liposomes by macrophages. Biochim Biophys Acta 1511:134–145.

Penault-Llorca F, Bertucci F, Adelaide J, Parc P, Coulier F, Jacquemier J, Birnbaum D, deLapeyriere O. 1995. Expression of FGF and FGF receptor genes in human breast cancer. Int J Cancer 61:170–176.

Qin M, Escuadro B, Sharma S, Batra RK. 2005. Gene transfer mediated by native versus fibroblast growth factor-retargeted adenoviral vectors into lung cancer cells. Am J Respir Cell Mol Biol 32:211–217.

Rusnati M, Urbinati C, Tanghetti E, Dell'Era P, Lortat-Jacob H, Presta M. 2002. Cell membrane GM1 ganglioside is a functional coreceptor for fibroblast growth factor 2. Proc Natl Acad Sci USA 99:4367–4372.

Safran M, Eisenstein M, Aviezer D, Yayon A. 2000. Oligomerization reduces heparin affinity but enhances receptor binding of fibroblast growth factor 2. Biochem J 345:107–113.

Sapra P, Allen TM. 2003. Ligand-targeted liposomal anticancer drugs. Prog Lipid Res 42:439–462.

Schubert F, Zettl H, Hafner W, Krauss G, Krausch G. 2003. Comparative thermodynamic analysis of DNA–protein interactions using surface plasmon resonance and fluorescence correlation spectroscopy. Biochemistry 42:10288–10294.

Sosnowski BA, Gonzalez AM, Chandler LA, Buechler YJ, Pierce GF, Baird A. 1996. Targeting DNA to cells with basic fibroblast growth factor (FGF2). J Biol Chem 271: 33647–33653.

Soulet F, Bailly K, Roga S, Lavigne AC, Amalric F, Bouche G. 2005. Exogenously added fibroblast growth factor 2 (FGF-2) to NIH3T3 cells interacts with nuclear ribosomal S6 kinase 2 (RSK2) in a cell cycle-dependent manner. J Biol Chem 280:25604–25610.

Stenlund P, Babcock GJ, Sodroski J, Myszka DG. 2003. Capture and reconstitution of G protein-coupled receptors on a biosensor surface. Anal Biochem 316:243–250.

Takanami I, Tanaka F, Hashizume T, Kikuchi K, Yamamoto Y, Yamamoto T, Kodaira S. 1996. The basic fibroblast growth factor and its receptor in pulmonary adenocarcinomas: An investigation of their expression as prognostic markers. Eur J Cancer 32:1504–1509.

Venkataraman G, Sasisekharan V, Herr AB, Ornitz DM, Waksman G, Cooney CL, Langer R, Sasisekharan R. 1996. Preferential self-association of basic fibroblast growth factor is stabilized by heparin during receptor dimerization and activation. Proc Natl Acad Sci USA 93:845–850.

Volm M, Koomagi R, Mattern J, Stammler G. 1997. Prognostic value of basic fibroblast growth factor and its receptor (FGFR-1) in patients with non-small cell lung carcinomas. Eur J Cancer 33:691–693.

Wegner GJ, Lee HJ, Marriott G, Corn RM. 2003. Fabrication of histidine-tagged fusion protein arrays for surface plasmon resonance imaging studies of protein–protein and protein–DNA interactions. Anal Chem 75:4740–4746.

Wu SJ, Chaiken I. 2004. Biosensor analysis of receptor-ligand interactions. Methods Mol Biol 249:93–110.

Yayon A, Aviezer D, Safran M, Gross JL, Heldman Y, Cabilly S, Givol D, Katchalski-Katzir E. 1993. Isolation of peptides that inhibit binding of basic fibroblast growth factor to its receptor from a random phage-epitope library. Proc Natl Acad Sci USA 90:10643–10647.

Ying W, Martineau D, Beitz J, Lappi DA, Baird A. 1994. Anti-B16-F10 melanoma activity of a basic fibroblast growth factor–saporin mitotoxin. Cancer 74:848–853.

FEBS Letters 580 (2006) 3706–3714

Intravenous administration of mannosylated cationic liposome/NFκB decoy complexes effectively prevent LPS-induced cytokine production in a murine liver failure model

Yuriko Higuchi, Shigeru Kawakami, Machiko Oka, Yoshiyuki Yabe, Fumiyoshi Yamashita, Mitsuru Hashida*

Department of Drug Delivery Research, Graduate School of Pharmaceutical Sciences, Kyoto University, 46-29 Yoshidashimoadachi-cho, Sakyo-ku, Kyoto 606-8501, Japan

Received 16 May 2006; accepted 25 May 2006

Available online 6 June 2006

Edited by Laszlo Nagy

Abstract The purpose of this study was to inhibit endotoxin induced cytokines production and liver injury by liver non-parenchymal cell (NPC) selective delivery of nuclear factor κB (NFκB) decoy using mannosylated cationic liposomes (Man-liposomes). In this study, we examined the distribution, inhibitory effect on cytokines production and ALT/AST of intravenously injected Man-liposome/NFκB decoy complex. Man-liposome/[^{32}P] NFκB decoy complexes mostly accumulated in the liver, preferentially in NPC. In a murine lipopolysaccharide-induced liver failure model, the production of tumor necrosis factor-α (TNFα), IFNγ, IL1-β, ALT and AST were effectively reduced by Man-liposome complexes. However, cationic or galactosylated cationic liposome complexes could not inhibit TNFα production.

Keywords: Mannosylated cationic liposome; Mannose receptor; NFκB decoy; Macrophage; Tumor necrosis factor-α

1. Introduction

Endotoxin syndrome is a particularly grave complication because bacteriologically proven infection occurs in up to 80% of patients with hepatic failure [1]. It is known that endotoxin syndrome, caused by infection of gram-negative bacteria, is a systemic inflammatory response mediated by several cytokines including tumor necrosis factor-α (TNFα), IL-1β, IFNγ, IL-12, etc., through nuclear factor κB (NFκB) activation in vivo [2]. Furthermore, increasing evidence indicates that Kupffer cells, hepatic resident macrophages, play a pivotal role in the production of the inflammatory cytokine response under a variety of stress conditions, such as hepatic failure, including viral infection [3,4]. Therefore, the prevention of cytokine overproduction by Kupffer cells would be an important factor for the treatment of endotoxin syndrome.

*Corresponding author. Fax: +81 75 753 4575.
E-mail address: hashidam@pharm.kyoto-u.ac.jp (M. Hashida).

Abbreviations: TNFα, tumor necrosis factor-α; LPS, lipopolysaccharide; NFκB, nuclear factor κB; PC, parenchymal cell; NPC, non-parenchymal cell

Several reports have demonstrated that NFκB activation in macrophages causes inflammatory cytokines and adhesion molecule production in a wide variety of types of inflammation and disease [5,6]. Recently Wrighton et al. [7] and Foxwell et al. [8] reported that adenoviral gene transfer of super-repressor IκB produced effective suppression of NFκB, however, the inflammatory reaction and high immunogenesity of the adenoviral vector itself posed a serious obstacle to in vivo therapy. In contrast, the decoy strategy has been developed and considered a useful tool as a new class of anti-gene strategy. In this NFκB decoy, double stranded oligonucleotides containing NFκB binding sequences, bind to activated-NFκB consequently inhibiting transcription by NFκB [9–11]. Therefore, the NFκB decoy approach enables us to treat diseases by suppression of target gene expression without high immunogenisity [12].

To establish NFκB decoy therapy, it is necessary to develop a Kupffer cell-targeting carrier for NFκB decoy to treat liver disease because of the low accumulation in Kupffer cells after intravenous injection of NFκB decoy [13]. As far as the liver-specific delivery of NFκB decoy is concerned, Ogushi et al. [14] recently demonstrated that NFκB decoy, transferred by fusigenic liposomes with hemagglutinating virus of Japan (HVJ liposomes) from the portal vein, effectively suppressed endotoxin-induced fatal liver injury in mice. However, intraportal injection is difficult in clinical situations because it needs a skilful surgical technique and increases the burden on the patient. Although intravenous injection is the most simple method, HVJ liposomes cannot accumulate in the liver following intravenous injection, because HVJ liposomes fuse to cells in a non-specific manner [15,16]. As a consequence, oligonucleotide is non-specifically delivered by HVJ liposomes to the lung, spleen and kidneys after intravenous injection [16]. In fact, Ogushi et al. achieved a therapeutic effect only by intraportal injection of HVJ liposomes not by intravenous injection. Moreover, because Kupffer cells account for only 15% of the total liver cells [17], non-specific fusion with HVJ liposomes would cause an increase in the NFκB decoy dose. Furthermore, preparing HVJ liposomes is complicated with irradiation to remove viral toxicity and centrifugation to remove free HVJ, etc. [18]. Therefore, a Kupffer cell-targeting carrier for NFκB decoy would lead to a more effective treatment for lipopolysaccharide (LPS) induced liver injury.

To develop a Kupffer cell-specific targeting carrier for NFκB decoy, receptor-mediated uptake is a promising

0014-5793/$32.00 © 2006 Published by Elsevier B.V. on behalf of the Federation of European Biochemical Societies.
doi:10.1016/j.febslet.2006.05.059

approach [19] because Kupffer cells are known to express large numbers of mannose receptors on their surface [17]. Recently we designed cholesten-5-yloxy-*N*-{4-[(1-imino-2-D-thiomannosyl-ethyl)-amino]butyl} formamide (Man-C4-Chol) to prepare mannosylated cationic liposomes (Man-liposomes) for mannose receptor-mediated plasmid DNA (pDNA) delivery [20–23]. Man-C4-Chol can be stably incorporated into liposomes and easily recognized by mannose receptors under in vivo conditions [24]. Furthermore, because Man-C4-Chol has an amino group for binding to pDNA via electrostatic interaction and a mannose residue for recognition by mannose receptors, a high density of mannose residues can be provided on the surface of liposome without affecting the binding ability of the cationic liposomes to pDNA [20]. Furthermore, we demonstrated that the highest gene expression observed for pDNA complexed with Man-liposomes via mannose receptor-mediated endocytosis [25].

Since NFκB decoy has anionic charges on its surface, we believe that NFκB decoy could form a complex with cationic liposome mediated by electrostatic interaction. In addition, since the size of NFκB decoy (20 base pairs) was more than 300-times smaller than pDNA (about 7000 base pairs), a large amount of NFκB decoy could form a complex with Man-liposomes. In this respect, a smaller amount of Man-liposomes could effectively deliver NFκB decoy compared with pDNA delivery. The reduction in the dose of carrier would be attractive for clinical therapy because of the reduced side-effects and low cost. The purpose of this study was to establish decoy therapy for endotoxin-induced liver disease. We developed a potential carrier for Kupffer cell targeting delivery of NFκB decoy after intravenous injection, demonstrating the first in vivo therapy by targeted delivery of NFκB decoy via intravenous injection. Results were compared with naked NFκB decoy and its complex with bare cationic liposomes.

2. Materials and methods

2.1. Materials

N-(4-aminoethyl) carbamic acid *tert*-butyl ester and *N*-[1-(2,3-dioleyloxy)propyl]-*n,n,n*-tri-methylammonium chloride (DOTMA) were purchased from Tokyo Kasei Kogyo Co. Ltd. (Tokyo, Japan). Dioleoylphosphatidylethanolamine (DOPE) was purchased from Avanti Polar Lipids Inc. (Alabaster, AL, USA). Cholesteryl chloroformate, heparin LPSs (from salmonella enterica serotype Minnesota Re 595) and collagenase were purchased from Sigma Chemicals Pty. Ltd. (St. Louis, MO, USA). Oligonucleotides (NFκB decoy: 5′-AGTTGAGGGGACTTTCCCAGGC-3′, 5′-GCCTGGGAAAGTCCCCTCAACT-3′; random decoy: 5′-TTGCCGTACCTGACTTAGCC-3′, 5′-GGCTAAGTCAGGTACGGCAA-3′) were purchased from Operon Biotechnologies Inc. (Tokyo, Japan). Ethylene glycol-bis(β-aminoethylether)-*N,N,N′,N′*-tetraacetic acid (EGTA), Clear-Sol I and cholesterol were purchased from Nacalai Tesque Inc. (Kyoto, Japan). MEGALABEL™ 5′-End Labeling Kit was purchased from Takara Bio Inc. (Shiga, Japan). Soluene-350 was purchased from Perkin–Elmer Inc. (Boston, MA, USA). NAP-5 column was purchased from Amersham Biosciences Co. (Piscatway, NJ, USA). Trypan blue was purchased from Invitrogen Co. (Grand Island, NY, USA). Mouse TNFα BD OptEIA™ ELISA Kit was purchased from Becton, Dickinson and Company (Mississauga, Canada). Fraction-PREP™ Nuclear/Cytosol Fraction Kit was purchased from BioVision Inc. (Mountain View, CA, USA). Transaminase C II test wako was purchased from Wako Pure Chemical Industries Ltd. (Osaka, Japan). Chemiluminescent NFκB Activation Assay Kit was purchased from Oxford Biomedical Research Inc. (Oxford, MI, USA).

2.2. Animals

Female ICR mice (5-week old, 22–24 g) or female C57BL/6 mice (6-week old, 18–20 g) were obtained from Shizuoka Agricultural Cooperative Association for Laboratory Animals (Shizuoka, Japan). All animal experiments were carried out in accordance with the Principles of Laboratory Animal Care as adopted and promulgated by the US National Institutes of Health and with the Guidelines for Animal Experiments of Kyoto University.

2.3. Radiophosphorylation of decoy oligonucleotides

Annealed NFκB decoy were labeled with [γ-^{32}P] ATP using MEGALABELTM 5′-End Labeling Kit with some modification as reported previously [13]. Briefly, oligonucleotides, [γ-^{32}P] ATP and T4 polynucleotide kinase were mixed in phosphorylation buffer. After 30 min incubation at 37 °C, the mixture was incubated for 10 min at 70 °C in order to inactivate T4 polynucleotide kinase. Then, the mixture was purified by gel chromatography using a NAP 5 column and eluted with 10 mM Tris–Cl and 1 mM EDTA (pH 8.0). The fractions containing derivatives were selected based on their radioactivity.

2.4. Synthesis of Man-C4-Chol

Man-C4-Chol was synthesized as reported previously [20]. Briefly, cholesteryl chloroformate and *N*-(4-aminobutyl)carbamic acid *tert*-butyl ester were reacted in chloroform for 24 h at room temperature. A solution of trifluoroacetic acid and chloroform was added dropwise and the mixture was stirred for 4 h at 4 °C. The solvent was evaporated to obtain *N*-(4-aminobutyl)-(cholesten-5-yloxyl)formamide which was then combined with 2-imino-2-methoxyethyl-1-thiomannoside and the mixture was stirred for 24 h at room temperature. After evaporation, the resultant material was suspended in water, dialyzed against distilled water for 48 h (12 kDa cut-off dialysis tubing), and then lyophilized. Gal-C4-Chol was also synthesized by the same method using galactose instead of mannose.

2.5. Preparation of liposomes and their complex with NFκB decoy

Man-liposomes, Gal-liposomes or DOTMA/cholesterol liposomes were prepared as reported previously [20]. Briefly, Man-C4-Chol, Gal-C4-Chol or DOTMA was mixed with DOPE or cholesterol, respectively, in chloroform at a molar ratio of and the mixture was dried, vacuum desiccated, and resuspended in sterile 5% dextrose. After hydration, the dispersion was sonicated for 10 min in a bath sonicator and then for 3 min in a tip sonicator to form liposomes.

The preparation of liposome/NFκB decoy complexes for in vivo use was carried out by the method of Kawakami et al. [25]. Equal volumes of NFκB decoy and stock liposome solution were diluted with 5% dextrose at room temperature. Then, the NFκB decoy solution was added rapidly to the liposome solution and the mixture was agitated rapidly by pumping it up and down twice in the pipet tip. The mixture was then left at room temperature for 30 min. The theoretical charge ratio of lipid/NFκB decoy was calculated as a molar ratio of Man-C4-Chol (monovalent) to a nucleotide unit (average molecular weight 330) [21,26,27].

The particle size of the liposomes and liposomes/NFκB decoy complexes were measured using dynamic light scattering spectrophotometer (LS-900, Otsuka Electronics, Osaka, Japan). The zeta potential of liposomes and liposome/NFκB decoy complexes were measured by Nano ZS (Malvern Instruments Ltd., Malvern, WR, UK).

2.6. In vivo distribution

In vivo distribution was examined as previously reported [13]. NFκB decoy complexed with liposomes in 300 μl 5% dextrose solution was intravenously injected into mice. Blood was collected from the vena cava at 1, 5, 10, 30, 60 min, and mice were killed at each collection time point. Liver, kidney, spleen, heart and lung were removed, washed with saline, blotted dry, and weighed. Immediately prior to blood collection, urine was also collected directly from the urinary bladder. 10 μl of blood and 200 μl of urine, and a small amount of each tissue were digested with Soluene-350 (0.7 μl for blood, urine and tissues) by incubation overnight at 54 °C. Following digestion, 0.2 ml isopropanol, 0.2 ml 30% hydroxyperoxide, 0.1 ml 5 M HCl, and 5.0 ml Clear-Sol I were added. The samples were stored overnight, and radioactivity was measured in a scintillation counter (LSA-500, Beckman, Tokyo, Japan).

2.7. Intrahepatic distribution

Intrahepatic distribution of [^{32}P] NFκB decoy complexed with Man-liposomes was determined as in our previous report [24]. Five minutes after intravenous injection of NFκB decoy, Man-liposome/NFκB decoy or cationic liposome/NFκB decoy complex, each mouse was anesthetized with diethyl ether and the liver was perfused with pre-perfusion buffer (Ca^{2+}, Mg^{2+}-free Hanks buffer, pH 7.4, containing 1000 U/L heparin and 0.19 g/L EGTA) for 6 min at 5 ml/min followed by Hanks buffer containing 5 mM $CaCl_2$ and 220 U/ml collagenase (Type I) (pH 7.4) for 6 min at 5 ml/min. After discontinuation of the perfusion, liver was excised and liver cells were dispersed in ice-cold Hanks-HEPES buffer. The cell suspension was filtered through cotton gauze, followed by centrifugation at 50 × *g* for 1 min at 4 °C. The pellet containing parenchymal cells (PC) was washed 4 times with ice-cold Hanks-HEPES buffer. The supernatant containing non-parenchymal cell (NPC) was collected and purified by centrifugation at 50 × *g* for 1 min at 4 °C (4 times). PC and NPC suspensions were centrifuged at 340 × *g* for 10 min. PC and NPC were then resuspended separately in ice-cold Hanks-HEPES buffer (final volume 2 ml). The cell number and viability were determined by the trypan blue exclusion method. The radioactivity of 500 μl of each cell suspension was measured by the same method as for the in vivo distribution.

2.8. Animal treatment protocol

For cytokine secretion assessment, blood was collected from ICR mice 1 h after intravenous injection of LPS (0.4 mg/kg). The blood was allowed to coagulate for 2–3 h at 0.4 °C and serum was isolated as the supernatant fraction following centrifugation at 2000 × *g* for 20 min. The serum samples were immediately stored at −80 °C. The amounts of TNFα, IL-1β and IFN-γ were analyzed using an Opti-EIA™ ELISA Kit according to the manufacturer's protocol. For severe liver injury model, C57BL/6 mice were injected intraperitoneally with LPS (0.05 mg/kg) and D-galactosamine (1000 mg/kg) in pyrogen-free saline. The blood was allowed to coagulate for 2–3 h at 4 °C and serum was isolated as the supernatant fraction following centrifugation at 2000 × *g* for 20 min. Serum ALT and AST were measured with transaminase C II test wako according to the manufacturer's protocol.

2.9. Enzyme immunoassay for determination of the amount of nuclear NFκB

Liver was removed, washed with ice-cold saline, and blotted dry. A small amount of liver was homogenized in phosphate-buffered saline. Pellets of cells were obtained by centrifugation at 500 × *g* for 2 min, and a nuclear extract was prepared using a Nuclear/Cytosol Fraction Kit. The amounts of NFκB in the nuclei were measured with an NFκB Activation Assay Kit according to the manufacturer's protocol.

2.10. Statistical analysis

Statistical comparisons were performed by Student's *t* test for two groups and one-way ANOVA for multiple groups. Post hoc multiple comparisons were made by using Turkey's test.

3. Results

3.1. Particle size and zeta potential of Man-liposomes and their complex with NFκB decoy

Table 1 summarizes the mean diameter and zeta potential of liposomes or liposome/NFκB decoy complex in 5% dextrose. The mean diameter of the Man-liposome/NFκB decoy complex was less than 100 nm. After forming a complex with NFκB decoy, the charge on the surface of Man-liposome/NFκB decoy complex slightly decreased and the mean diameter was not changed.

Table 1
The mean particle sizes and zeta potential of liposome and liposome/NFκB decoy complexes

	Particle size (nm)	Zeta potential (mV)
Man-liposome	64.6 ± 1.70	61.4 ± 0.91
Man-liposome complex	61.6 ± 1.58	54.7 ± 0.60

3.2. Man-liposome/NFκB decoy complex rapidly and highly accumulated in liver after intravenous injection

Fig. 1 shows the time-courses of the radioactivity in blood, kidney, spleen, liver, lung, muscle and heart after intravenous injection of naked [^{32}P] NFκB decoy or [^{32}P] NFκB decoy complexed with Man-liposomes or cationic liposomes. Ten minutes after the intravenous injection of Man-liposome/[^{32}P] NFκB decoy complex, about 80% of the dose accumulated in the liver. However, naked [^{32}P] NFκB decoy was rapidly excreted in the urine and gradually accumulated in the kidney. Also, cationic liposome/[^{32}P] NFκB decoy complex gradually accumulated in the liver after rapid accumulation in the lung.

3.3. Man-liposome/NFκB decoy complex preferentially taken up by NPC

After intravenous injection of Man-liposome/[^{32}P] NFκB decoy complex, the radioactivity in the liver was preferentially recovered from the NPC fraction with the radioactivity ratio of NPC to PC (NPC/PC ratio on a cell-number basis) in the liver being approximately 2.6 (Fig. 2). In contrast, naked [^{32}P] NFκB decoy had an NPC/PC ratio of 0.66 (Fig. 2) and the cationic liposome/[^{32}P] NFκB decoy complex had NPC/PC ratio of 0.75 (Fig. 2). The total liver accumulation of Man-liposome/[^{32}P] NFκB decoy complex was higher than that of naked [^{32}P] NFκB decoy.

3.4. Man-liposome/NFκB decoy complex effectively suppressed inflammatory cytokine production

The serum concentration of TNFα was assessed using ELISA to confirm that NFκB decoy complexed with Man-liposomes effectively suppressed the production of inflammatory cytokines induced by LPS in vivo (Fig. 3). After intravenous injection of LPS, the highest serum concentration of TNFα was observed at 1 h (data not shown). Control mice were only treated with LPS for 1 h. A dose-dependence in the suppression effect of Man-liposome/NFκB decoy complex was observed (Fig. 3A).

Thirty micrograms of NFκB decoy complexed with Man-liposomes markedly inhibited the production of TNFα in serum compared LPS alone. However, the same amount of NFκB decoy complexed with cationic liposomes or Gal-liposomes could not inhibit TNFα production (Fig. 3B). Moreover, 30 μg of a random decoy of almost the same size but with no NFκB binding sequence had no inhibitory effect on TNFα production (Fig. 3C). These results indicated that the inhibitory effect of TNFα production depended on the sequence of the NFκB decoy.

The serum concentrations of IL-1β and IFNγ were also assayed by ELISA (Fig. 4). The serum level of IL-1β and IFNγ induced by LPS was significantly suppressed by intravenous administration of Man-liposome/NFκB decoy complex (Fig. 4A and B). IFNγ is partly produced in response to LPS-induced inflammatory cytokines (TNFα, IL-12, etc.). Therefore, the inhibition of IFNγ by Man-liposome/NFκB decoy complex indicated secondary inhibition following to the inhibition of the upstream cytokines.

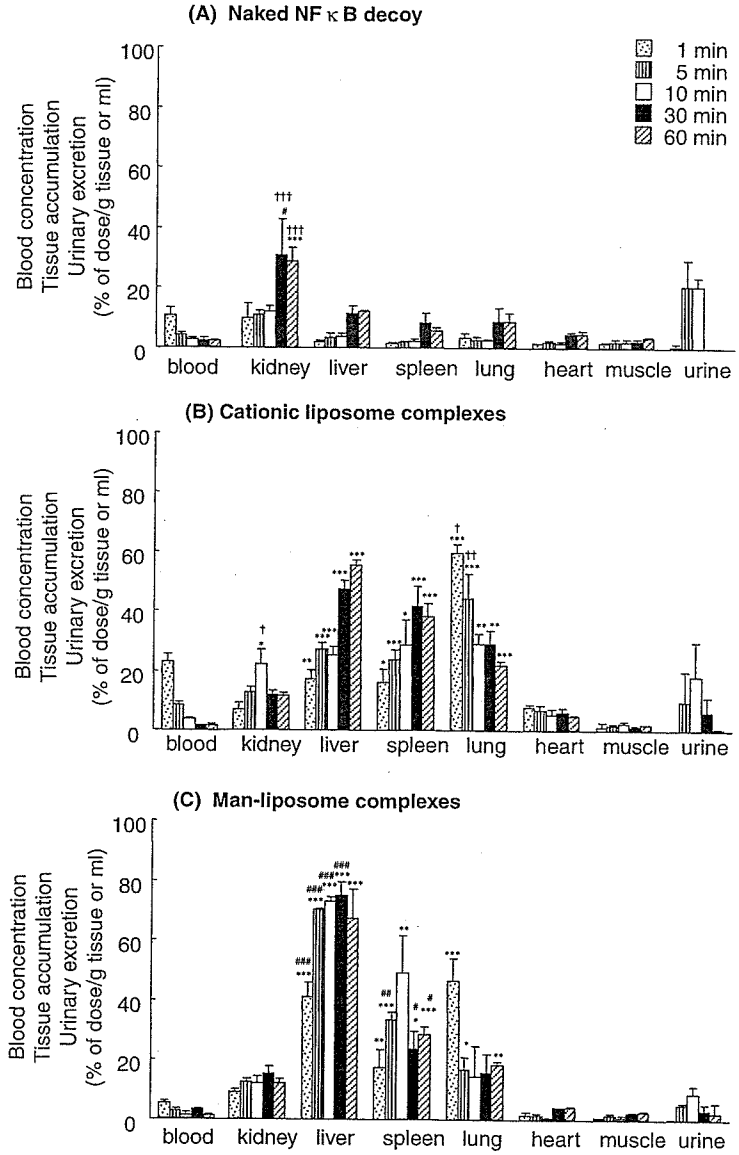

Fig. 1. Blood concentration, tissue accumulation and urinary excretion of ^{32}P-labeled naked NFκB decoy (A), cationic liposome/^{32}P-labeled NFκB decoy complex (B) and Man-liposome/^{32}P-labeled NFκB decoy complex (C) after intravenous injection into mice. ^{32}P-labeled NFκB decoy was complexed with mannosylated liposomes or cationic liposomes at a charge ratio of 2.3:1.0 (+:−). Radioactivity was determined in blood, liver, lung, spleen, kidney, heart, muscle and urine after 1, 5, 10, 30 and 60 min. Each value represents the mean ± S.D. ($n = 3$). Significant difference: $^{***}P < 0.001$, $^{**}P < 0.01$, $^{*}P < 0.05$ vs. (naked NFκB decoy); $^{\#\#\#}P < 0.001$, $^{\#\#}P < 0.01$, $^{\#}P < 0.05$ vs. (cationic liposome complexes); and $^{\dagger\dagger\dagger}P < 0.001$, $^{\dagger\dagger}P < 0.01$, $^{\dagger}P < 0.05$ vs. (Man-liposome complexes).

3.5. Man-liposome/NFκB decoy complex effectively prevents severe liver injury

ALT or AST measured in serum provide an index of hepatocyte integrity. Leakage of ALT and AST into the extracellular compartment and a subsequent rise in serum reflect hepatocytes damage. These enzymes are significantly elevated at liver damage caused by LPS induced inflammatory cytokines. Only LPS treatment with ICR mice did not caused significantly rise serum ALT and AST level (data not shown). Therefore, LPS and D-(+)-galactosamine treated C57BL/6 mice were used to determine therapeutic effect of Man-liposome/NFκB decoy complex for liver injury. The serum activity of ALT and AST increased after administration of LPS and D-(+)-galactosamine, which indicated severe liver injury. Although naked NFκB decoy did not prevent liver injury, Man-liposome/NFκB decoy complex significantly inhibit increase of ALT and AST level in the serum (Fig. 5). These results indicated Man-liposome/NFκB decoy complex could prevent LPS caused liver injury.

3.6. Man-liposome/NFκB decoy complex effectively prevents NFκB activation in nuclei

In response to inflammatory stimuli, IκB protein degraded and allowed NFκB to translocate into the nucleus to initiate gene expression of inflammatory cytokines. The amount of activated NFκB in the nuclei was measured by enzyme immu-